Atmos. Chem. Phys. Discuss., 8, 15537–15594, 2008
www.atmos-chem-phys-discuss.net/8/15537/2008/

Atmospheric Chemistry and Physics Discussions

Dispersion of traffic-related exhaust particles near the Berlin urban motorway: estimation of fleet emission factors

W. Birmili[1], B. Alaviippola[2,1], D. Hinneburg[1], O. Knoth[1], T. Tuch[1,3], J. Kleefeld-Borken[4,*], and A. Schacht[4]

[1]Leibniz Institute for Tropospheric Research (IfT), Permoserstrasse 15, 04318 Leipzig, Germany
[2]Finnish Meteorological Institute (FMI), P.O. Box 503, 00101 Helsinki, Finland
[3]Helmholtz Center for Environmental Research – UfZ, Permoserstrasse 15, 04318 Leipzig, Germany
[4]German Aerospace Center (DLR), Transportation Research, Rutherfordstrasse 2, 12489 Berlin, Germany
[*]now at: International Institute for Applied Systems Analysis, Schlossplatz 1, 2361 Laxenburg, Austria

Received: 23 May 2008 – Accepted: 3 July 2008 – Published: 15 August 2008

Correspondence to: W. Birmili (birmili@tropos.de)

Published by Copernicus Publications on behalf of the European Geosciences Union.

Abstract

Atmospheric particle number size distributions of airborne particles (diameter range 10–500 nm) were measured over ten weeks at three sites in the vicinity of the A100 urban motorway in Berlin, Germany. The A100 carries about 180 000 vehicles on a weekday, and roadside particle size distributions showed a number maximum between 20 and 60 nm clearly related to the motorway emissions.

The average total number concentration at roadside was 28 000 cm^{-3} with a total range between 1200 and 168 000 cm^{-3}. At distances of 80 and 400 m from the motorway the concentrations decreased to mean levels of 11 000 and 9 000 cm^{-3}, respectively. An obstacle-resolving dispersion model was applied to simulate the 3-D flow field and traffic tracer transport in the urban environment around the motorway. By inverse modelling, vehicle emission factors were derived, representative of a relative share of 6% lorry-like vehicles, and a driving speed of about 80 $km\,h^{-1}$. Three different calculation approaches were compared, which differ in the choice of the experimental winds driving the flow simulation. The average emission factor per vehicle was $2.1(\pm0.2)\cdot10^{14}$ km^{-1} for particle number and $0.077(\pm0.01)\cdot10^{14}$ $cm^3\,km^{-1}$ for particle volume. Regression analysis suggested that lorry-like vehicles emit 116 (± 21) times more particulate number than passenger car-like vehicles, and that lorry-like vehicles account for about 91% of particulate number emissions on weekdays. Our work highlights the increasing applicability of 3-D flow models in urban microscale environments and their usefulness in determining traffic emission factors.

1 Introduction

Clear associations have been found between ambient particular matter (PM) and adverse health effects in humans (Künzli et al., 2000; Pope et al., 2002). It is a hypothesis that the health effects observed in broad parts of the population may be caused by a particular sub-fraction of PM rather than total PM mass (HEI, 2002). Epidemiologi-

ACPD

8, 15537–15594, 2008

cal evidence has related respiratory disease with ultrafine particles, i.e. with diameters < 100 nm (Schwartz et al., 1996; Peters et al., 1997), or with traffic-related emissions in general (Brunekreef et al., 1997; Kim et al., 2004).

A number of arguments point towards the possible induction of health effects by traffic aerosols: The mere small size of ultrafine particles could lead to a deep penetration into the lung, and subsequent irritations in the alveolar region, where ambient air is in exchange with the blood circulation (Seaton et al., 1995). Furthermore, particulate traffic emissions contain high numbers of insoluble particles, such as diesel soot (Weingartner et al., 1997; Rose et al., 2006). Such particles are only poorly removed from the lung. Engine emissions tend to contain organic toxins (PAHs) and a myriad of other so far unidentified micropollutants (e.g., Spurny, 1999; Gelencser, 2004).

Motor vehicles inject a wide spectrum of particles into the atmosphere. While coarse particles may be emitted directly through break wear, and indirectly by road dust resuspension, fine particles are primarily emitted in the form of combustion engine exhaust. Modern engines tend to emit less particle mass, but this is not necessarily true for particle number (Ntziachristos et al., 2004). Most of particle number, especially in gasoline vehicle emissions, has been found in the ultrafine size range (Kean et al., 2003). Recent measurements of a representative cross-section of European passenger cars by Samaras et al. (2005) during the EU Commission Particulates Programme confirmed that diesel engines without particulate diesel filter emit significantly more PM mass, and also particle number than conventional gasoline vehicles. Mass emissions from gasoline cars still vary considerably with engine technology. Mass emissions from conventional gasoline engines are about three orders of magnitude lower than diesel cars without diesel particulate filter, but direct injection gasoline engines (Euro III norm) are only one order of magnitude lower. Dynamometer tests showed that the diameter of maximum particle number concentration of diesel exhaust particles lies mostly in the region between 60 and 80 nm, however, depending on the engine technology and the state of driving (Ntziachristos et al., 2004; Samaras et al., 2005).

Diesel particulate filters seem to reduce the emissions of diesel cars to those compa-

rable to conventional gasoline cars (Burtscher, 2005). Heavy duty engines were found to behave similar to passenger car diesel engines, and showed decreasing mass emission rates with improving engine technology (Mayer et al., 2007). As the particulate mass emission rate increases in proportion with the engine power, heavy duty vehicles may emit the multiple of emissions of a conventional passenger car. Nucleation mode particles < 50 nm tend to be created by all engine types especially at high driving speeds (i.e. high engine loads) and with sulphur-rich fuel. Even vehicles equipped with diesel particulate filters may emit particle numbers considerably above ambient levels (Ntziachristos et al., 2004; Samaras et al., 2005).

Dynamometer experiments highlighted that the concentration of the nucleation mode depends on the dilution process of the sampled exhaust gas (Kittelson, 1998; Mathis et al., 2004). When vehicles are driven on real roads, new particles may be formed downstream the exhaust pipe, i.e. when hot exhaust gas cools down and causes nucleation of sulfuric as well as unburnt organic fuel compounds. This effect depends on temperature as well as vehicle-induced turbulence and can not necessarily be reproduced by dynamometer measurements. It is evident that the role of aerosol dynamical processes grows with increasing proximity to the exit of the exhaust pipe (Pohjola et al., 2003; Zhang and Wexler, 2004). The ubiquity of traffic-related nucleation particles and their relevance to outdoor concentrations have been confirmed by many observations in roadside environments (Zhu and Hinds, 2002; Wehner et al., 2002; Charron and Harrison, 2003; Hussein et al., 2004; Rosenbohm et al., 2005; Voigtländer et al., 2006).

In order to capture the full impact of traffic-generated particles on the environment, atmospheric experiments near traffic sources are required, particularly in combination with a numerical assessment of particle dispersion and transport as well as aerosol dynamical processes. Numerous works have dealt with pollutant dispersal in simplistic configurations of urban landscapes, such as street canyons, and relatively accurate descriptions for these scenarios have been developed and experimentally verified (Vardoulakis et al., 2003; Holmes and Morawska, 2006). While most of the local fluid mechanical processes in an urban landscape are understood, the most appropriate

framework to study and quantify dispersal in the case of extended, more irregular topographies is less clear (Britter and Hanna, 2003). In several cases, however, three dimensional fluid dynamics models have already been applied to describe pollutant dispersal in irregular urban landscapes (Schlünzen et al., 2003; Wissink et al., 2005).

This paper reports on ambient measurements of sub-μm particle size distributions in the vicinity of the A100 urban motorway in Berlin, Germany. We apply a 3-D micrometeorological model to simulate dispersion of traffic emissions downwind the motorway. The particle measurements are combined with vehicle counts and meteorological dilution factors to derive real-world and size-segregated emission factors for the entire fleet, as well as passenger cars and lorries separately.

2 Experimental

2.1 The A100 motorway field experiment

Sub-μm particle size distributions were measured between July and September 2005 during 10 weeks in the vicinity of the A100 Berlin urban motorway. Measurements were carried out several kilometres west of Berlin's city centre in the district of Westend (52° 31′ N, 13° 17′ E, 55 m above sea level), an area densely build-up with multi-storey residential buildings (see Fig. 1). Particle size distributions were measured simultaneously at three measurement sites with different distances and in different directions from the motorway. The A100 motorway carries about 180 000 vehicles on 6 lanes per working day and traverses the area through a traffic corridor about 100 m wide that includes the Berlin circular urban railway. Although the motorway is the overwhelming source of traffic-generated aerosols, several secondary roads lead through the area, notably the Spandauer Damm street, which crosses the motorway perpendicularly in east-westerly direction. It will be shown later, however, that emissions from these streets are expected to play a minor role only.

ACPD
8, 15537–15594, 2008

2.2 Particle measurement sites

The roadside measurement site was the one in closest proximity to the motorway (Fig. 1). As the measurement site had been previously used by the Berlin city council as a part of the communal air quality monitoring system, it had already a pre-existing cabin infrastructure. Immediately to the north of the roadside site, slip roads lead to the Spandauer Damm avenue that crosses the motorway further north. At the roadside site the aerosol inlet was located 4 m off the pavement of the motorway horizontally, and 6 m vertically. Size distribution measurements at the roadside site lasted from 29 June until 5 September 2005. The auxiliary measurements included local wind speed and wind direction using a cup anemometer as well as ambient temperature, relative humidity and air pressure on hourly averages.

The first background measurement site (simply termed "background site" in the following) was located about 80 m east of the motorway, therefore serving as a site more downstream of the source than the roadside site. South of the background site, the two three-lane carriageways of the A100 split, and the easterly (northbound) carriageway is conducted on a flyover in order to pass over the Berlin circular urban railway. Therefore, the background site was located approximately 10 m below the more closely situated carriageway. Between the motorway and the background site, electrified suburban trains circulate as the only possible additional source of particles. Measurements were performed from inside a temporarily located measurement trailer with an aerosol inlet 6 m above the ground. Size distribution measurements lasted from 30 June until 2 September 2005. Further measurements at the site included wind speed and wind direction with an ultrasonic anemometer (model USA-1, Metek Inc., Elmshorn, Germany).

A second background measurement site (simply dubbed "distant background site" in the following) was located about 400 m distant from the motorway, and designed to be a background station to both other sites. Measurements were made from inside a laboratory van and included particle size distribution, nitrogen oxide and dioxide and

ACPD
8, 15537–15594, 2008

meteorological measurements. Size distribution measurements at the distant background site lasted between 5 July until 10 August 2005.

Additional data resources include the wind speed and wind direction measured by the German Meteorological Service (DWD) at the airport Berlin-Tegel, located about 4 km north of the measurement area (Fig. 1c). The Tegel wind data is recorded at a height of 10 m above the ground in an undisturbed area and therefore utilized as an indicator of the large scale wind.

2.3 Particle mobility spectrometers

Ambient particle number size distributions were recorded continuously at each of the measurement sites. The instrumentation used included two main types of particle mobility spectrometers. The background site was equipped with a Twin Differential Mobility Particle Sizer (TDMPS) covering a particle diameter range between 3 and 900 nm. The TDMPS is a custom made instrument similar to that described in Birmili et al. (1999). Briefly, two Vienna type differential mobility analysers (Winklmayr et al., 1991) were deployed having centre rod lengths of 11 and 28 cm, respectively. The sheath air in the two DMAs was circulated in a closed loop using spin-regulated blowers. The sheath/aerosol flow ratio in the two DMAs was 20/2.0 and 5.0/0.5 l min^{-1}, respectively. The relative humidity inside the system was kept under 30%.

The roadside and distant background sites, on the other hand, were equipped with Scanning Mobility Particle Sizers (SMPS model 3080 with long DMA; TSI Inc., St Paul, USA) operated at a sheath air ratio of 5.0/0.5 l min^{-1}. Both systems used a model 3010 condensation particle counter operated at the standard flow rate 1.0 l min^{-1}. The particle size range covered by these instruments was 10–500 nm. The relative humidity inside the SMPS instruments could not be actively controlled, but was estimated to be within a range of 20–40%.

To ensure a maximum comparability of the size distributions determined at different sites, direct comparison experiments using the same ambient sample aerosol were performed over several days before and after the campaign. Among the systematic de-

ACPD
8, 15537–15594, 2008

viations identified between different instruments were a) the measured overall particle concentration and b) the instrumental number concentration response as a function of particle diameter. Both of these effects were corrected for each instrument when evaluating the final data. Since the TDMPS instrument is least affected by particle losses in the ultrafine range (< 20 nm) the data measured by both TSI instruments was corrected upwards. We estimate that the corrected particle concentrations inferred from each instrument across the size spectrum 10–600 nm are comparable within ± 10%.

2.4 Traffic counts

The traffic on the A100 motorway is routinely counted about one kilometre north of the particle sampling site. The detectors TT292 of ASIM combine radar, ultrasound and passive infrared monitoring to count the vehicles on each lane separately. Vehicles are identified by shape and classified into two length classes, shorter and longer than 6.5 m. The shorter length class is comprised of motorcycles, passenger cars, vans and minibuses, sport utility vehicles and delivery vans. The longer length class comprises lorries, busses, and vehicle combinations (i.e. including trailers). This size information is in the following used as an approximation to distinguish between "passenger car-like vehicles" (PC) and "lorry like vehicles" (LDVs and HDVs). We use data for the period between 29 June and 5 September 2005 here.

The detectors simultaneously measured the number and speed of the vehicles passing during each second. An accuracy of classification between 98 and 99% is given for both length classes on a minute and hourly average. Misdetection may occur due to lane crossing and in case of congested traffic; then the size resolution may be flawed. This traffic counting site is the most accurate and closest to the roadside and background measurement sites. However, there is a motorway exit and access point at Spandauer Damm in between. Hence the number of southbound vehicles passing the roadside and background measurement sites equals the number of vehicles at the traffic counting site minus the vehicles having exited plus the vehicles entering at Spandauer Damm. For the northbound traffic the conditions are inverse. In order to

establish the balance of entering and leaving vehicles, we therefore counted the traffic manually at that site during a short follow-up experiment (27 March 2007).

The distance between traffic counting site and particle measurement site implies a slight time lag: At an average speed of $80 \pm 20\,\mathrm{km\,h^{-1}}$ southbound vehicles pass the traffic counting site about $45 \pm 15\,\mathrm{s}$ earlier than the particle measurement sites; northbound they are counted this time later. Since emission factors of the vehicular fleet will later be derived on the basis of one hour data averages, this short delay can safely be neglected.

3 Experimental results

3.1 Traffic counts

Between 28 June and 6 August 2005 about 180 000±17 000 vehicles passed the traffic counting facility on an average weekday (Table 1). The overall share of "lorry like" vehicles was about 6%. Almost 90% of all vehicles passed in the period from 05:00 to 21:00 (CET), with peaks of more than 10 000 vehicles per hour between 06:30 and 09:00, and 15:30 and 18:30, respectively.

On Saturdays the total number of "car like" vehicles was at about 80% of the weekday level while "lorry like" vehicles dropped to 40% of that level. The peak levels occurred now around midday (between 13:15 and 15:15) and a significantly higher portion of the traffic occurred during night time. The average Sunday was marked by still lower traffic volume at about 70% and 30% of the average weekday level for "car like" and "lorry like" vehicles, respectively.

Relative maxima in traffic occurred from 13:10 to 15:40 and between 17:00 and 19:00, too. Again, a higher portion of the traffic occurred during night times. Figure 2a shows the typical diurnal cycle with a very sharp increase for the morning rush hour, a long and high level of the traffic volume during the day and long decrease from 18:00 onwards. The share of "lorry like" vehicles, notably medium and heavy duty trucks as

ACPD
8, 15537–15594, 2008

well as busses, was on average 6% on working days, 3.3% on Saturdays and 2.5% on Sundays. The ratio of "lorry like" to passenger cars is shown in Fig. 2b. As can be seen, this ratio changes between 1.5 and 15%, and has its lowest values on Saturdays and Sundays.

On working days the ratio is about 8% during daytime. Importantly, this ratio stays relatively constant between 07:00 and 17:00, i.e., the period that covers the major amount of daily traffic. A pronounced maximum of 15% occurs during the early morning hours (02:00 and 04:00). This maximum ratio is certainly an effect of low numbers, and only valid for this short time period: Passenger car numbers are at an absolute minimum at this time, while lorry traffic is about to rise. On Saturdays the diurnal variation is similar to working days whereas on Sundays the number of "lorry like" vehicles is low throughout the day. The latter is partially a result of legal traffic restrictions, which prohibit lorry traffic on Sundays except for perishable goods.

About 1200 to 1500 vehicles per hour left and entered the motorway at Spandauer Damm during daytime on 27 March 2007. This corresponds to about 12–15% of the vehicles on the motorway. North-South entering and exiting traffic was imbalanced by a few 100 vehicles per hour. We transfer this point measurement to estimate the total traffic volume at the particle measuring site, i.e. a few tenth of meters south of Spandauer Damm. During daytime we have to increase the hourly traffic volume by about 300 vehicles, i.e. 3% of the total hourly traffic flow. The fluctuation in the time series and any longitudinal correlations derived is even less. We have no data for the night time but do not expect any significant distortions.

The speed limit is 80 km h^{-1} on that section of the motorway, but in reality the traffic density is the limiting factor for the speed. The measured driving speed fluctuates diurnally between 75 and 90 km h^{-1} with higher speeds during night time when the traffic volume is lower.

ACPD
8, 15537–15594, 2008

3.2 Particle concentrations

In the proximity of the Berlin urban motorway we found exceptionally high levels of ambient particle number concentrations. At roadside, total particle number (D_p>10 nm) exceeded 100 000 cm^{-3} on many occasions. A maximum value of 168 000 cm^{-3} was recorded during the morning peak traffic hours ("rush hours"), while the lowest concentration 1200 cm^{-3} occurred after midnight. The average total particle concentration for the whole measurement period was 28 000 cm^{-3}. The background site, located 80 m east of the motorway, featured considerably lower number concentration, 11 000 cm^{-3} on average and varying between 1700 and 70 000 cm^{-3}. The distant background site, located 400 m downwind the traffic source, was characterised by the lowest total particle concentration of the three sites, 9000 cm^{-3} on the average, and varying in the range of 1800–60 000 cm^{-3}.

Figure 3 shows the diurnal evolution of the particle number size distribution at the three urban measurement sites on Tuesday, 12 July 2005. One can clearly see the influence of traffic emissions at roadside, which features by far higher number concentrations than the background and distant background sites. While the concentrations at roadside are influenced by the traffic throughout the day, its influence was the greatest between 04:00 h, i.e. the onset of motorway traffic (Fig. 2), and 12:00 h on this day. Although the two background sites are separated by a few major streets over a distance of about one km the evolution of their number size distributions in Fig. 3 appears amazingly similar. On 12 July the winds came from the north, i.e. parallel to the motorway. The coincidence of individual aerosol plumes detected around 03:00, 06:00, 11:00, 13:00, 17:00, and 22:00 h in Fig. 3b-c illustrates the high spatial homogeneity of particle size distributions in the urban background around the motorway. Figure 4 depicts average particle size distributions at the roadside and the background sites for the rush hour period 07:00–09:00 h. The influence of motorway emissions is most pronounced across the wide size interval between 10 and 200 nm.

ACPD
8, 15537–15594, 2008

3.3 One-week case studies

To illustrate the impact of traffic density and meteorological parameters on the measured concentrations, two one-week periods, each ranging from a Monday to a Sunday, are examined in detail. Week 1 covered the period between 11 and 17 July (Day of year 192- -199), while Week 2 spanned from 8 to 14 August (Day 220–227). Figure 5 illustrates the observed variations of meteorological as well as particle and traffic parameters.

The beginning of week 1 was characterised by high pressure influence, so that the daily maximum temperatures rose to 30°C with clear diurnal variations (Fig. 5a). From Monday to Thursday the Sun shone 12–15 h per day and also the weekend was sunny. The prevailing wind direction was north, and the wind speed exhibited a distinct diurnal cycle with higher winds during the day. The week was intercepted by a weather change on Friday, when the wind briefly turned to westerly directions associated with a cold front and heavy rainfall in the night towards Saturday. The traffic volume followed the typical profiles indicated earlier (Fig. 2a) and showed little variations between Monday to Thursday. According to the traffic speed measurements, there were only few short traffic jams during this week. From Monday to Friday the roadside site featured morning peaks in total particle concentration of more than 100 000 cm^{-3}, but decreasing concentrations to about 40 000 cm^{-3} in the afternoon under similar traffic volumes. Prime reasons for this concentration decrease are an increasing wind speed and improved conditions for vertical dilution during mid-day. On the weekend, the overall concentrations were substantially lower due to smaller traffic volumes and wind blowing from the west. In summary, the case study of week 1 illustrates that the experimental observations are well repeatable under steady meteorological conditions.

Week 2, in contrast, was characterised by low pressure influence and, for summer, quite low daily maximum temperatures (15–20°C) with no clear diurnal cycle (Fig. 5b). The Sun shone only on Monday and Friday, with clouds prevailing during the rest of the week. The wind blew steadily from the west with relatively high wind speeds from

ACPD
8, 15537–15594, 2008

Tuesday to Thursday. Occasionally, the traffic volume was lower than usual due to traffic jams with minimum driving speed of less than 40 km h^{-1} in the afternoons on Tuesday–Friday. During week 2 the particle number concentrations were on generally low level, seldom exceeding 50 000 cm^{-3} at roadside. Is becomes obvious that the westerly wind placed the roadside site upwind of the motorway, and accounted for the low roadside concentrations. During a few periods of stagnant air (local wind speeds near zero), particle concentrations at the background site were able to increase beyond 20 000 cm^{-3}. The case study of week 2 shows that under meteorological conditions favourable for dilution, ambient particle concentrations stayed low.

3.4 Diurnal cycle

The strong periodicity of the traffic source leads to clear diurnal variation of the measured particle concentrations: Fig. 6 presents average diurnal cycles for particle number concentrations on workdays. Here, the concentrations for each particle diameter are normalised by the average levels at the background site. A first feature is that the traffic influence increases with decreasing particle size. During the rush hour, the concentrations at roadside reach two times the background value for particles >300 nm but more than 9 times the background value for particles <20 nm (Fig. 6). This behaviour is closely related to the fingerprint of the traffic emissions in the size distribution (Fig. 4). At the background site, a diurnal trend can be seen for all particle sizes as well as a result of a changing urban background. During the weekend (data not shown), the diurnal patterns are less pronounced as a result of a diverging traffic patter.

3.5 Lognormal parameters

To provide a more generally accessible version of the data, lognormal distributions were fitted to selected particle size distributions. Similar to earlier works (Morawska et al., 1999; Birmili et al., 2001; Hussein et al., 2005), three particle modes were found to be sufficient in parameterising the observations. The smallest mode was dubbed “young

ACPD
8, 15537–15594, 2008

Aitken mode" and believed to originate from the nucleation of unburnt fuel components in the wake of the vehicles. Table 2 summarises the lognormal modal parameters of the size distributions modes at the roadside, background and distant background sites. The size distributions used were the 25th, 50th, 75th, 95th, and 99th percentile distributions simulating different degrees of pollution influence. To provide comparable modes, the spread parameter σ was held fixed to the values indicated in the table. Table 2 demonstrates that the influence of traffic emissions is most pronounced in the Young Aitken mode (centered at 18 nm), and decreases towards the Aitken (53–81 nm) and the accumulation mode (134–208 nm). This means that the impact of traffic emissions on locally measured particle number increases in inverse proportion to particle size.

4 Dispersion modelling

4.1 Modelling technique

The micro-scale atmospheric model ASAM (All-Scale Atmospheric Model; Hinneburg and Knoth, 2005) is used to simulate the three-dimensional dispersion of an inert tracer, i.e. without physical and chemical transformations, in the surrounding of the measuring sites. The prognostic, non-hydrostatic, and inelastic model solves the conservation equations for momentum, turbulent kinetic energy and dissipation, potential temperature, moist constituents as well as inert tracers by third-order implicit techniques. The model adopts the standard k-ϵ-turbulence model of first-order closure with shear and buoyant production terms and the constant-flux approach on the walls and the surface.

In ASAM the orography as well as all obstacles, i.e. buildings, bridges, and ramps, are explicitly represented by completely or partially (with inclined surfaces) filled grid cells in a rectangular Cartesian z-coordinate system (not terrain-following). Figure 7 shows the relatively complex model domain with a raised surface as well as an outstanding building block immediately west of the motorway. The lowered northern part of the motorway passes under a long bridge (Spandauer Damm), while the southern

ACPD
8, 15537–15594, 2008

part splits in two disjoined lanes. The model was applied to a region of 500 m×500 m with 5 m horizontal grid spacing. Its vertical extension was 100 m with the vertical grid resolution varying from 2 m in the obstacle layer to 10 m at the model top.

Traffic emissions were implemented as constant area sources in grid cells adjacent to the lanes of the motorway. Neutral temperature profiles and a uniform roughness of 0.10 m for the surface and the walls were assumed. A total of ten simulations was performed with different directions of the driving wind, which is fixed at the top of the model domain (h=100 m). Open conditions were set for all variables on the lateral boundaries.

In order to generalise the simulation results in terms of wind speeds and concentrations, scaling relations with the driving wind speed U and the line source intensity Q were applied (Palmgren et al., 1999; Ketzel et al., 2003). The normalised local wind speed u^* (non-dimensional) is defined as:

$$u^* = \frac{u}{U}, \tag{1}$$

with u being the local wind speed and U the large scale wind speed far from the surface (h=100 m). The normalised local concentration c^* (non-dimensional) is defined as:

$$c^* = \frac{c \cdot U \cdot H}{Q}, \tag{2}$$

where c is the local tracer concentration (in m^{-3}) induced by the emission source, Q the line source intensity in $m^{-1}\,s^{-1}$, and H the characteristic obstacle height (concretely $H = 40$ m, the maximum height of the street canyon). Q indicates the number of particles emitted in one second per one metre of road. An important assumption is that the normalised local wind speeds u^* and concentrations c^* are nearly independent of the magnitude of U and Q, leaving the wind direction as the remaining main source of variability.

ACPD
8, 15537–15594, 2008

4.2 Simulation results

Figure 8 presents the simulated wind fields together with the distributions of the normalised concentrations for the four main directions of the driving wind. Red colours illustrate the dispersion of motorway emissions within the modelling domain. The layer shown corresponds to the height of the roadside measurement site, ca. 13 m above ground level and about 9 m above the motorway. Grid cells in this layer that are covered by buildings or the orographically varying surface appear in gray. Table 4 compiles the simulation results for a more comprehensive set of 10 wind directions.

A major conclusion from Fig. 8 is that the impact of traffic emissions on the concentrations at the roadside measurement site ("R") varies greatly with wind direction. The concentrations are predicted to be high under northerly winds (D=0°), moderate under easterly winds (90°), and low under southerly winds (180°). Although the roadside site is located upstream of the motorway, ASAM predicts relatively large concentrations under easterly winds (270°) because of the leeward vertical and horizontal vortices above the motorway (Fig. 8). A vertical cross-section in east-west direction (not shown) suggested a vertical vortex behind the tall building block, associated with small wind speeds and low exchange conditions. Because minor changes in the position of the receptor point led to large variations in the predicted concentrations, it is our impression that under westerly winds the roadside site ("R") is located critically near this horizontal vortex with its associated high concentration gradients.

An overall look at the tracer concentrations of the background measurement site ("B" in Fig. 8) showed only marginal contributions from the motorway except under westerly winds (270°), which place the background site downwind the motorway. Simulations similar to those in Fig. 8 were performed for the dispersal of the Spandauer Damm street traffic emissions (Fig. 7). These simulations suggested only a marginal influence of the Spandauer Damm street emissions on the concentrations at the roadside and background sites compared to the A100 motorway.

ACPD
8, 15537–15594, 2008

4.3 Validation of simulated wind parameters

The local wind speed measurements were used to validate the performance of our 3-D dispersion model. Figure 9a compares the simulated and experimental wind directions for the roadside and background sites. All wind directions are plotted against the large scale wind direction (Tegel airport), which is driving the simulation. A main result is that the wind direction at the background site is reproduced relatively accurately by the model. This is not surprising given the relatively unobstructed position of that site ("B" in Fig. 8).

At the roadside site, an agreement between simulations and experiment can be found for the majority of wind directions, with the notable exception of westerly and northwesterly winds (270–315° in Fig. 9a). While the simulation predicts the roadside site to lie in the vortex counterflow behind the large building block (Fig. 8) the experimental values plead for a close coupling of the large-scale and local winds.

This deviation between simulations and experiment is likely a result of the complex local topography around the roadside site, which can only be reproduced in the model with a high degree of simplification. It is an intriguing feature of the model simulation that it ascribes a higher degree of uncertainty to the simulated wind directions from the westerly sector; in fact, the model recognizes that this flow situation leads to unstable results for the given configuration of westerly winds at the roadside site.

The comparison of simulated and experimental wind speeds in Fig. 9a–b yields similar conclusions. While the ratio between modelled and measured wind speed is within 0.5–1.0 at the background site, the results are more diverse at the roadside site: While a fair agreement between modeled and measured wind speed (ratio between 0.5 and 1.0) was achieved for northerly and easterly wind directions (338–330°; 0–145°), the comparison is more erratic for southerly and westerly winds.

In summary, the three-dimensional flow simulation reproduces the experimental wind directions and speeds at the background site (40 m west of the motorway) reasonably well. For the roadside site, a reasonable agreement was found for northerly and east-

ACPD
8, 15537–15594, 2008

erly wind directions (338–360° and 0–145°). For southerly and westerly winds, the simulations do not correspond equally well to the observations. As a consequence, observations from these wind sectors will be excluded when deriving vehicle emission factors below.

4.4 Vehicle emission factors from inverse modelling

We now combine the dispersion simulation results from Sect. 4 and the experimental data from Sect. 3 to derive vehicle emission factors for the A100 motorway. Inverse modelling refers to a methodology that allows to conclude on the intensity of pollution sources based on simulated transport to a receptor site and concentration measurements there (Ketzel et al., 2003). Since our transport simulation does not include physical and chemical particle transformations, the calculation of an emission factor requires the particles to be inert (i.e. non-reactive) during the transport between the source and the receptor point. Coagulation is an important process in highly concentrated aerosols, and we tested the life-time of aerosol particles at the roadside site with respect to coagulation (see Appendix). The life-times were on the scale of 10 minutes and more for average conditions, so that the derived emission factors can be taken representative for the emission flux through the envelope of the motorway as a line source.

The inverse modelling approach yields the emission factor E (in $\mathrm{veh}^{-1}\,\mathrm{km}^{-1}$), which indicates the number of particles emitted by the vehicle fleet per kilometre driven under the prevailing traffic flow conditions. E is defined as:

$$E = \frac{Q}{M}, \tag{3}$$

with Q being the line source intensity (Sect. 4.1) and M the traffic volume in $\mathrm{veh\,s}^{-1}$. Particle dispersion downwind the traffic source is described by the dilution factor F,

ACPD
8, 15537–15594, 2008

having units of s m^{-2}:

$$F = \frac{c}{Q} \tag{4}$$

Here, c is the roadside increment concentration in particles m^{-3}. For the roadside site, this roadside increment was calculated as c(roadside)-c(background). For the background site, which also shows a diurnal, albeit much weaker concentration cycle (Fig. 6) we used the minimum of its own concentrations across a moving 24 h window as a best estimate for its background concentration. When combining Eqs. 2 and 4 the dilution factor F can be reformulated as:

$$F = \frac{c^*}{U \cdot H} \tag{5}$$

In this equation, U can be replaced by the experimental $\overline{U}$. Since U refers to the driving wind of the simulation at a height of 100 m, its experimental replacement $\overline{U}$ needs to correspond to the same height. $\overline{U}$ was determined from wind speed measurements at Tegel airport (10 m above the surface) by scaling the measured value according to simulated vertical wind profiles. A scaling factor $\overline{U}$(100 m)/$\overline{U}$(10 m) of 1.5 was chosen, which was calculated on the basis of a logarithmic wind profile and an estimated roughness length of 0.1 m at Tegel airport.

After combining Eqs. 3, 4 and 5, importing the experimental data, and substituting experimental $\overline{c}^*$ with modelled c^* the emission factor E becomes:

$$E = \frac{\overline{c} \cdot \overline{U} \cdot H}{\overline{M} \cdot c^*}, \tag{6}$$

where the barred variables represent experimental values. In this equation the emission factor is calculated as a function of the large scale experimental wind.

ACPD
8, 15537–15594, 2008

To check the reliability of the substitution of U by $\overline{U}$, we analysed a scaling relationship between measured and modelled wind speeds by defining a scaling constant:

$$\eta = \frac{\overline{u}}{\overline{U}} \cdot \frac{U}{u}. \quad (7)$$

Here, $\overline{u}/\overline{U}$ is the ratio of the experimental local and large scale wind speeds and u/U the corresponding modelled wind speed ratio. η expresses the degree of correspondence between experiment and simulation and will, in general, depend on several factors including wind direction. The case η=1 implies the same ratio of local to large scale winds both in the experiment and the simulation. To determine values of η that are representative of distinct wind sectors, linear trend lines were fitted to scatter plots of $\overline{u}$ against $\overline{U}$. To eliminate any bias caused by calm wind situations, only data with Tegel wind speeds $> 2\,\mathrm{m\,s^{-1}}$ were accepted.

In practice, the following values of η were determined: For the roadside site, an average of 0.63 (total range 0.30–1.19) was calculated, i.e., the experimental wind is on average slower than predicted by the simulation. For the background site, η was determined to be 0.30 (total range 0.23–0.38), i.e. the experimental winds were disproportionately lower than the simulated ones. These results suggest that it remains an important issue to verify a three-dimensional dispersion model by local wind speed measurements. With the above mentioned amendments and by using Eqs. 1, 6 and 7, the emission factor E can be described as:

$$E = \frac{\overline{c} \cdot \overline{u}}{\overline{M} \cdot (c^* u^*) \cdot \eta} \quad (8)$$

where $c^* u^*$ is the product of the normalised variables c^* and u^* (see Table 4). Eq. 8 is a variant of Eq. 6 where eventual wind-directional dependencies of the relationship between the local and large scale wind speeds are accounted for.

ACPD
8, 15537–15594, 2008

A third approach for E is to use Eqs. 1 and 6 before importing the experimental data, and finally to associate experimental $\overline{c}^*\overline{u}^*$ with modelled c^*u^*

$$E = \frac{\overline{c} \cdot \overline{u} \cdot H}{\overline{M} \cdot (c^* u^*)} \tag{9}$$

The difference between Eqs. 6 and 9 is that the product c^*u^* is, in contrast to c^*, independent of the particular choice of U. It is worth to point out that the local experimental wind speed is used in Eq. 9 rather than the large scale wind speed, as in Eq. 6. In Eq. 9 the local experimental wind is therefore assumed to be representative for the pollutant dispersal rather than the large scale wind.

Fleet emission factors were calculated as a function of experimental and simulated parameters according to Eqs. 6, 8 and 9. Due to restricted computing time, u^*, c^* and c^*u^* were calculated for 10 discrete wind directions only (Table 4). To provide values as a continuous function of large-scale wind direction, they were linearly interpolated.

For the determination of average emission factors, some sections of the data set were removed. This concerned 50% of the data occurring in calm wind conditions, defined as Tegel wind speeds below $2\,\mathrm{m\,s^{-1}}$. We assume that under calm winds the transport model will not represent the local dispersion conditions accurately. This may be due to a weak coupling between large-scale and local winds, and the increasing dominance of vehicle-induced turbulence with decreasing wind speed, which is neglected in the model.

In addition, the emission factors based on roadside measurements were aggregated for the wind sector 330–150°only, which correspond to a situation of the receptor site downwind of the motorway. Under southwesterly winds (160–240°) the model predicts only little motorway contributions. The wind sector 250–320°was excluded because the local simulated and measured wind speeds and wind directions differed most (Sect. 4.3). For the background site, emission factors were calculated for the wind sector 160–330°which likewise places the receptor site downwind of the motorway.

5 Experimental vehicle emission factors

5.1 Fleet emissions on weekdays

Figure 10 shows average diurnal cycles of the particle number emission factor using the three different approaches introduced in Sect. 4.4. Figure 10a is based on the evaluation of the concentration difference between roadside and background site, while Fig. 10b is based on background site measurements only — taking a floating 24 h-minimum value as a background measure. In Fig. 10a, particle number emission factors E in a range $1–4 \cdot 10^{14}$ veh^{-1} km^{-1} (wind direction 330–150°only) can be seen depending on the time of day and the calculation approach used. The values derived from Eq. 6 – based on a coupling of the model to the large-scale wind, are comparable to those from Eq. 9, which are based on a coupling to the local wind. Eq. 8 tends to produce the highest emission factors.

Figure 10b presents emission factors (wind direction 160–330°) based on background site measurements only. The day-time values derived from Eqs. 6 and 8 range between $1 – 2 \cdot 10^{14}$ veh^{-1} km^{-1} and are of similar magnitude like the values in Fig. 10b. This agreement is, in fact, surprising because generally, a much weaker signal from the motorway is picked up at the background site only (cf. Fig. 5). The emission factors derived from Eq. 9, however, are lower by a factor of more than three. This leads to the conclusion that associating the simulated and measured c^*u^*, as is done in Eq. 9 is not appropriate. We explain the problem by the overestimation of the local wind speed at the background site by the model (cf. Fig. 9b). Values derived from Eq. 9 using background site values are therefore not discussed further.

All approaches share three visible stages in the diurnal cycle (Fig. 10): high values at night (21:00–07:00), medium values during mid-day 07:00–13:00), and lower values in the afternoon (13:00–21:00). Several possible explanations for these stages are outlined. First, the emission factor is expected to be a function of the fleet composition, which varies throughout the day (Fig. 2b). On weekdays, the ratio between lorry-like and passenger car-like vehicles reaches a maximum of 15% at 03:00 h, which coin-

ACPD
8, 15537–15594, 2008

cides with the maximum in E around that time (Fig. 10). However, the overall traffic volumes and consequently the pollutant concentration are also the lowest during the night. When small values of $\overline{c}$ and M are divided in Eqs. 6, 8 and 9, the result will accordingly be more uncertain. Third, rolling traffic causes a significant portion of air turbulence (e.g., Vachon et al., 2002). This is currently not accounted for in our dispersion model but is expected to correlate with the traffic volume. It is currently unclear what causes the drop in the emission factor around 13:00.

Table 5 compiles the particle number emission factors on weekdays based on the concentration difference between roadside and background site.

5.2 Weekend effects and lorry/passenger car split

The diurnal cycle of the motorway emission factor was also calculated for weekends because these values provide to be useful when examining the effects of a changing fleet composition. Figure 11 compares the diurnal cycles of E on weekdays, Saturdays and Sundays for the roadside site based on Eq. 8. It can be seen that between 08:00 and 16:00, the weekend values of E are substantially lower than on weekdays. From our analysis it is evident that this difference is mainly related to differences in the share of lorry-like vehicles.

This difference was evaluated to determine the relative shares of lorry-like and passenger car-like vehicles. Assuming that the total emission factor E_{total} can be described as a superposition of the factors of lorry-like (E_l) and passenger-car like (E_p) vehicles weighted after their relative shares n_l and n_p of the traffic volume and using $n_p = 1 - n_l$ we obtain

$$E_{\text{total}} = (E_l - E_p) \cdot n_l + E_p. \quad (10)$$

Following this equation E_{total} is plotted against n_l in Fig. 11 (inset) for data points ranging between 08:00 and 12:00. The slope of the fitted line is interpreted as $E_l - E_p$, while its y-intercept corresponds to E_p. For the time window 07:00–16:00 and data points from weekdays and Saturdays (Sunday data had to be omitted due to an

in sufficient statistical data base) particle number emission factors of $10\,(\pm 1.5)$ and $0.09\,(\pm 0.06)\cdot 10^{14}\,\mathrm{veh}^{-1}\,\mathrm{km}^{-1}$ were determined for lorry-like and passenger-car like vehicles, respectively. It is worth to note that E_l could be derived with greater confidence than E_p because the latter depended more sensitively on the propagation of experimental noise in Eq. 10. A further implication of the results is that on the Berlin urban motorway, lorry-like vehicles emit $116\,(\pm 21)$ times more particle number than passenger-car like vehicles, or that lorry-like vehicles account for 83% of day-time particulate number emissions on Saturdays and 91% on weekdays.

We acknowledge that these results might also by biased by the driving behaviour. On weekends, the traffic was always flowing at an average speed around $80\,\mathrm{km\,h}^{-1}$. During weekdays, limited periods of traffic congestion (<2 h/day) could occasionally be observed, which led to average speed as low as 50–60 $\mathrm{km\,h}^{-1}$. Although their effect on the calculated emission factors are hard to quantify, it is assumed that slower speeds will increase the experimental emission factor as a result of the vehicles' longer residence within the surroundings of the measurement site. Consequently, the emission factors for lorry-like vehicles have to be regarded as an upper estimate, and those for passenger car-like vehicles as a lower estimate (cf. their sensitivity in Fig. 11/inset).

5.3 Emission factor size distributions

The data was also used to determine size distributions of the emission factor. The necessary conditions used for determining representative values were, again, wind from the sector 330–150°(roadside site downstream the motorway), a sufficient wind speed (Tegel wind speed $>2\,\mathrm{m\,s}^{-1}$), and the time window 07:00–16:00 (sufficient traffic volume). Figure 12 depicts the size distribution of E obtained under these conditions. Due to the apparent bimodality of the distributions, two lognormal modes with geometric mean diameters of 17 and 71 nm were fitted. These modes are associated with the nucleation and soot modes commonly seen in tailpipe emissions (Kittelson, 1998), with the nucleation mode being generated in the free atmosphere downwind of the tailpile.

ACPD
8, 15537–15594, 2008

6 Discussion

Vehicular emission factors were determined by quantifying the 3-D micrometeorological dilution between the motorway as a source and two receptor points. While this is similar to the practice of Gaussian plume models or street canyon dispersion models, the method is more different from the evaluation of the dilution in tunnel measurements or a calculation of emission factors by relating particle to gaseous tracer concentrations.

A useful byproduct of our method is that, like every dispersion model, the 3-D simulation pictures the impact of traffic emissions in the surroundings of the motorway (Sect. 4.2). Concentration maps such as Fig. 8 can be useful for an assessment of the exposure of local residents to particles and gases originating from the motorway.

A sensitive issue in the quantification of the emission factor has been the choice of the experimental wind speeds that served to drive the flow model (Sect. 4.4). Three options were pursued, using the large-scale wind (Tegel airport; Eq. 6), the local wind at the receptor sites (Eq. 9), and a more elaborate version of the first option, eliminating possible wind-directional bias due to the inhomogeneous terrain (Eq. 8). When using the large-scale wind, the accuracy of the calculation is limited by the ability of the flow model to describe the microscale airflow between the source and the receptor points, though the derived values also rely on the correct choice of roughness length when generating the large scale wind speed (h=100 m) from the near-surface measurements at Tegel (h=10 m).

The use of local winds to drive the flow model avoids several of these uncertainties, but relies more specifically on the model's ability to correctly simulate local wind speeds and directions. This ability was considered satisfactory for the surroundings of the roadside site in the wind sector 330–150°(i.e. downwind the motorway), but unsatisfactory for the wind speed at the background site albeit the wind direction could be simulated well there (Sect. 4.3). Our general impression is that the three approaches produce comparable results for the roadside site (Fig. 10a), whereas Eq. 9 seems to

ACPD
8, 15537–15594, 2008

generate unrealistically low emission factors when applied to data from our background site (Fig. 10b). For the aggregation of the final fleet emission factors we selected data calculated by Eq. 8, and based on subtracting background from roadside concentrations.

Another issue of uncertainty is our assumption on the emitted particles being inert during the transport. Calculations on the life-time of 18 nm-particles (see Appendix) suggest that coagulation is not critical in reducing particle number concentration over the scale of minutes, once the particles have left the envelope of the motorway. Aerosol transformation simulations (Zhang et al., 2004) have suggested that particle growth and shrinkage, as well as changes in chemical composition occur downwind of traffic sources as a result of the rapid dilution. Our tentative assumption here is that most of the "tailpipe-to-ambient" dilution process has passed once the particles are detected at the roadside site near the A100 motorway. Further changes in particle number downwind due to aerosol dynamics are therefore expected to be minor, and the derived emission factors are, in fact, representative for the flux of aerosol particles exiting through the envelope of the motorway at a distance of 6 m off the kerbside.

What vehicular fleet are the emission factors derived in this paper representative for? According to HBEFA (2004) the share of diesel vehicles among passenger cars was 26% in Germany in 2004. A field study in the surroundings of Berlin, however, determined a smaller fraction of diesel cars of 20% only among passenger vehicles (LUA, 2006). (For vans and lorries the shares of diesel-driven vehicles were 86% and 100%, respectively HBEFA, 2004). For the A100 motorway in 2005, we assume that the share of diesel vehicles among passenger cars was between the reported values of 20 and 26%. Currently, the number of diesel vehicles among newly licensed cars is about 50% in Germany and hence, the share of diesel vehicles in the fleet is constantly mounting. However, the fitting of diesel cars and HDVs with particulate filters is underway and expected to reduce particulate mass but also number emissions (Ban-Weiss et al., 2008). Therefore, the values derived in our work can be regarded as representative of the state in 2005.

It is also worth to recall that our measurements took place during summer (average temperature 18°C, relative humidity 50–90%, average cloud cover 50%), and that the emission factors derived are representative for such meteorological conditions only. We are aware that for thermodynamic reasons the particulate number emission factor may increase with decreasing temperature, as indicated by other works (Olivares et al., 2007; Jamriska et al., 2008).

Table 6, finally, compiles numerous works in which particulate emission factors were determined from stationary near-road measurements, focussing on roads where the traffic is free flowing and travelling at speeds above 80 km^{-1} h^{-1}. A more general survey of traffic-derived emission factors was given by Jones and Harrison (2006).

Figure 13 visualises the trend that can be recognised between the mixed fleet emission factors and the fraction of HDVs, based on numbers from the upper section of Table 6. It appears that higher experimental cut-off sizes yield lower emission factors, which is not surprising in view of the substantial particle concentrations emitted in the diameter range between 3 and 30 nm, where the experimental cut-off diameters of the particle mobility spectrometers and/or particle counters can be found.

Further differences between the different studies can be explained by systematic differences between the different calculation methods, different seasons in which measurements took place, and deviations in the structure of the vehicle fleets. European vehicle fleets usually contain a substantial fraction of diesel-driven LDVs while in Australia, their number is negligeable (Morawska et al., 2005). Further non-comparability may result from differences in the methods of classifying vehicles into HDVs, LDVs, and an eventual intermediate class (transport vehicles, “vans”), which is usually accomplished by vehicle length in optical detection systems.

7 Conclusions

Measurements of atmospheric particle number size distributions in the vicinity of the A100 urban motorway in Berlin, Germany, yielded average total particle concentrations

of 28 000 cm^{-3} (1200–168 000 cm^{-3}) at roadside (6 m off the kerbside), and around 11 000 and 9000 cm^{-3} at two distances of 80 and 400 m downwind, respectively. The measured particle numbers depended highly on the traffic volume, but also sensitively on the meteorological conditions including wind speed and wind direction. While the general features of the observations agree with the findings of many former studies, it is the large volume of traffic (180 000 vehicles on a workday at a share of 6% lorry-like vehicles) in a densely populated area which make the location of the A100 a relevant showcase to study the dispersion of traffic-related particles in a complex urban landscape.

An obstacle resolving dispersion model (ASAM) was used to simulate the 3-D flow field as well as the transport and dilution of a traffic-emitted tracer in an area with 500 m horizontal box size. Great care was taken with the accurate spatial representation of the obstacles (horizontal resolution 5 m) in the area and the motorway as a traffic source. The simulation was able to explain the overall spatio-temporal trend of the measured particle size distributions with a notable exception of westerly flow, where the situation of real obstacles was the most complicated. By a validation of the model with the experimentally measured local winds, time periods could be identified when the receptor points were in a well-defined flow situation downwind of the motorway as the traffic source.

Using the method of inverse modelling, vehicle emission factors were derived. The average number emission factor per vehicle was $2.1(\pm0.2)\cdot10^{14}$ km^{-1} for the particle size range 10–500 nm. A corresponding factor of $0.077(\pm0.01)\cdot10^{14}$ cm^3 km^{-1} could be determined for the particulate volume. After fitting two lognormal modes to the emission factor number size distribution, values of 1.5(±0.2) and $3.3(\pm0.3)\cdot10^{14}$ km^{-1} were obtained for the soot mode and the nucleation mode, respectively. By combining weekday and weekend observations, we were able to delineate the contributions caused by lorry-like and passenger car-like vehicles, suggesting that that lorry-like vehicles emit 116 (± 21) times more particulate number than passenger car-like vehicles, and that lorry-like vehicles account for about 91% of particulate number emissions on

ACPD
8, 15537–15594, 2008

weekdays.

An issue relevant to the quantification of the emission factor was the choice of the experimental wind speeds that served to drive the flow model. Three options were pursued, using either a large-scale wind, local winds at the receptor sites, or an alternative version of the first approach eliminating possible wind-directional bias. Our general conclusion is that the three approaches produce comparable results when applied to a traffic-induced contribution derived by subtracting background site measurements from roadside measurements.

It has been an unusual approach to determine emission factors by taking into account meteorological dilution calculated from an explicit 3-D flow model. Previous works have often relied on parameterised box or plume models, the consideration of air dilution in tunnels, or a coupling to gaseous tracers (CO, NO_x). A certain advantage of our method is that the 3-D simulation can quantify the effects of additional minor roadways in the surroundings, and picture the spatial impact of traffic emissions in the entire urban area adjacent to the motorway. Meanwhile we are aware of the model's current limitations, such as the negligence of traffic-induced turbulence as well as physical and chemical transformations of the emitted particles. We anticipate that the method will be further developed and deployed in similar traffic settings when studying traffic-related particle emissions over the years to come.

Appendix A

Lifetime of small particles due to coagulation

Among all sub-μm particles, especially nano-sized particles are subject to enhanced loss and deposition processes. We examined the life-time of 18 nm-particles (i.e. the diameter of maximum number concentration at roadside) against coagulation with bigger particles. The life-time was calculated using a box model and coagulation by Brownian diffusion in the transition regime (Seinfeld and Pandis, 1998). Because the particle

size range encompassed by our measurements encompassed only 10–500 nm, calculations were also performed with the addition of a coarse particle mode ($N = 5\,\mathrm{cm}^{-3}$; $\sigma = 1.72$; $D_{g0} = 1.2\,\mu\mathrm{m}$). (The calculated life-times proved, however, insensitive towards the presence of this particle mode.)

The life-times of 18 nm-particles with respect to Brownian coagulation are shown in Table 7. $t(0.90\,N_0)$ corresponds to the time after which particle concentration N_0 has dropped to 90% of its initial value. $t(0.75\,N_0)$ and $t(0.50\,N_0)$ describe the decay of particle number to 75 and 50%, respectively. The model size distributions of the 50th, 75th, 95th, and 99th percentile correspond to the tri-modal distributions from Table 2. An additional model size distribution "Percentile 99, YA·10" was added, in which the concentration of the young Aitken mode was artificially increased by a factor of 10 in order to simulate less diluted concentrations closer to the tailpipe. Calculations were made for a low ambient relative humidity scenario, simulated by a hygroscopic growth factor (GF) of 1, and high ambient relative humidity scenario, simulated by GF=1.4. Hygroscopic growth of bigger particles increases the coagulation sink, and the GF used corresponds to a typical value found for continental accumulation mode particles at 90% relative humidity (Lehmann et al., 2005). In Table 7 it can be seen that under typical roadside conditions (50th, 75th and 95th percentile), the shortest life-time $t(0.90\,N_0)$ is 6 min (under humid conditions), so that the effect of coagulation of 18 nm-particles can be safely neglected for transport times of several minutes.

Acknowledgements. This work was supported by the German Environmental Agency (UBA) project UFOPLAN 204-42-204/03. We thank Dieter Bake from UBA Berlin for his generous support during the preparation and conduction of the field experiment, and his help regarding the supply of auxiliary data. André Sonntag and Korinna König assisted with the particle measurements during the campaign in Berlin, while Ibro Pandzo and Simone Warwel measured and evaluated the traffic volumes. Birgitta Alaviippola acknowledges support by the EU Marie Curie host fellowship (contract number EVK2-CT-2002-57005), coordinated by Prof. Alfred Wiedensohler (IfT Leipzig). Parts of the data evaluation for this paper were conducted within the European Integrated project on Aerosol Cloud Climate and Air Quality Interactions (EUCAARI), coordinated by the University of Helsinki, Finland.

References

Abu-Allaban, M., Coloumb, W., Gertler, A., et al.: Exhaust particle size distribution measurement at the Tuscarora mountain tunnel, Aerosol Sci. Technol., 36, 771–789, 2002.

Ban-Weiss, G. A., McLaughlin, J. P., Harley, R. A., et al.: Long-term changes in emissions of nitrogen oxides and particulate matter from on-road gasoline and diesel vehicles, Atmos. Env., 42, 220–232, 2008. 15562

Birmili, W., Stratmann, F., and Wiedensohler, A.: Design of a DMA-Based Size Spectrometer for a Large Particle Size Range and Stable Operation, J. Aerosol Sci., 30, 549–553, 1999. 15543

Birmili, W., Wiedensohler, A., Heintzenberg, J., and Lehmann, K.: Atmospheric Particle Number Size Distribution in Central Europe: Statistical Relations to Air Masses and Meteorology, J. Geophys. Res., 106, D23, 32 005–32 018, 2001. 15549

Britter, R. and Hanna, S.: Flow and Dispersion in Urban Areas, Annual Rev. Fluid Mech., 35, 469–496, 2003. 15541

Brunekreef, B., Janssen, N., de Hartog, J., Harssema, H., Knape, M., and van Vliet, P.: Air Pollution from Truck Traffic and Lung Function in Children Living near Motorways, Epidemiology, 8, 298–303, 1997. 15539

Burtscher, H.: Physical characterization of particulate emissions from diesel engines: a review, J. Aerosol Sci., 36, 896–932, 2005. 15540

Charron, A. and Harrison, R.: Primary particle formation from vehicle emissions during exhaust dilution in the roadside atmosphere, Atmos. Env., 37, 4109–4119, 2003. 15540

Corsmeier, U., Imhof, D., Kohler, M., et al.: Comparison of measured and model-calculated real-world traffic emissions, Atmos Env., 39, 5760–5775, 2005.

Gelencser, A.: Carbonaceous Aerosol, Springer, Berlin, 2004. 15539

Gramotnev, G., Brown, R., Ristovski, Z., Hitchins, J., and Morawska, L.: Determination of average emission factors for vehicles on a busy road, Atmos. Env., 37, 465–474, 2003.

HBEFA: The Handbook Emission Factors for Road Transport, INFRAS, Bern, Switzerland, 2.1 edition, 2004. 15562

HEI: Understanding the health effects of components of the particulate matter mix: progress and next steps, Tech. Rep. 4, Health Effects Institute, Boston, MA, 2002. 15538

Hinneburg, D. and Knoth, O.: Non-dissipative cloud transport in Eulerian grid models by the volume-of-fluid (VOF) method, Atmos. Env., 39, 4321–4330, 2005. 15550

Holmes, N. and Morawska, L.: A review of dispersion modelling and its application to the dispersion of particles: An overview of different dispersion models available, Atmos. Env., 40, 5902–5928, 2006. 15540

Hueglin, C., Buchmann, B., and Weber, R.: Long-term observation of real-world road traffic emission factors on a motorway in Switzerland, Atmos. Env., 40, 3696–3709, 2006.

Hussein, T., Puustinen, A., Aalto, P., Mäkelä, J., Hämeri, K., and Kulmala, M.: Urban aerosol number size distributions, Atmos. Chem. Phys, 4, 391–411, 2004. 15540

Hussein, T., Haämeri, K., Aalto, P., Paatero, P., and Kulmala, M.: Modal structure and spatial-temporal variations of urban and suburban aerosols in Helsinki, Finland, Atmos. Env., 39, 1655–1668, 2005. 15549

Imhof, D., Weingartner, E., Ordóñez, C., Gehrig, R., Hill, M., Buchmann, B., and Baltensperger, U.: Real-World Emission Factors of Fine and Ultrafine Aerosol Particles for Different Traffic Situations in Switzerland, Env. Sci. Technol., 39, 8341–8350, 2005.

Imhof, D., Weingartner, E., Prévôt, A., Ordóñez, C., Kurtenbach, R., et al.: Aerosol and NO_x emission factors and submicron particle number size distributions in two road tunnels with different traffic regimes, Atmos. Chem. Phys, 6, 2215–2230, 2006.

Jamriska, M., Morawska, L., and Mergernse, K.: The effect of temperature and humidity on size segregated traffic exhaust particle emissions, Atmos. Env., 42, 2369–2382, 2008. 15563

Janhäll, S. and Hallquist, M.: A Novel Method for Determination of Size-Resolved, Submicrometer Particle Traffic Emission Factors, Env. Sci. Technol., 39, 7609–7615, 2005.

Jones, A. M. and Harrison, R. M.: Estimation of the emission factors of particle number and mass fractions from traffic at a site where mean vehicle speeds vary over short distances, Atmos. Env., 40, 7125–7137, 2006. 15563

Kean, A., Harley, R., Littlejohn, D., and Kendall, G.: Effects of vehicle speed and engine load on motor vehicle emissions, Env. Sci. Technol., 37, 3739–3746, 2003. 15539

Ketzel, M., Wahlin, P., Berkowicz, R., and Palmgren, F.: Particle and trace gas emission factors under urban driving conditions in Copenhagen based on street and roof-level observations, Atmos. Env., 37, 2735–2749, 2003. 15551, 15554

Kim, J., Smorodinsky, S., Lipsett, M., Singer, B., Hodgson, A., and Ostro, B.: Traffic-related Air Pollution near Busy Roads: The East Bay Children's Respiratory Health Study, Am. J. Resp. Crit. Care Med., 170, 520–526, 2004. 15539

Kittelson, D.: Engines and Nanoparticles: A Review, J. Aerosol Sci., 29, 575–588, 1998. 15540, 15560

Kristensson, A., Johansson, C., Westerholm, R., Swietlicki, E., Gidhagen, L., Wideqvist, U., and Vesely, V.: Real-world traffic emission factors of gases and particles measured in a road tunnel in Stockholm, Sweden, Atmos. Env., 38, 657–673, 2004.

Künzli, N., Kaiser, R., Medina, S., Studnicka, M., Chanel, O., et al.: Public-health impact of outdoor and traffic-related air pollution: a European assessment, Lancet, 356, 795–801, 2000. 15538

Lehmann, K., Massling, A., Tilgner, A., Mertes, S., Galgon, D., and Wiedensohler, A.: Size-resolved soluble volume fractions of submicrometer particles in air masses of different character, Atmos. Env., 39, 4257–4266, 2005. 15566

LUA: Luftreinhalte-/Aktionsplan Bernau bei Berlin – Ermittlung emissionsrelevanter Parameter über die Erfassung von Kfz-Kennzeichen, 105, Landesumweltamt Brandenburg, Potsdam, Germany, 2006. 15562

Mathis, U., Ristimäki, J., Mohr, M., Keskinen, J., Ntziachristos, L., Samaras, Z., and Mikkanen, P.: Sampling Conditions for the Measurement of Nucleation Mode Particles, Aerosol Sci. Technol., 38, 1149–1160, 2004. 15540

Mayer, A., Kasper, M., Mosimann, T., Legerer, F., Czerwinski, J., Emmenegger, L., Mohn, J., Ulrich, A., and Kirchen, P.: Nanoparticle-emission of EURO 4 and EURO 5 HDV compared to EURO 3 with and without DPF, SAE transactions, 1, 1–9, 2007. 15540

Morawska, L., Thomas, S., Jamriska, M., and Johnson, G.: The Modality of Particle Size Distributions of Environmental Aerosols, Atmos. Env., 33, 4401–4411, 1999. 15549

Morawska, L., Jamriska, M., Thomas, S., et al.: Quantification of Particle Number Emission Factors for Motor Vehicles from On-Road Measurements, Env. Sci. Technol., 39, 9130–9139, 2005. 15563

Ntziachristos, L., Mamakos, A., Samaras, Z., Mathis, U., Mohr, M., et al.: Overview of the european Particulates project on the characterization of exhaust particulate emissions from road vehicles: Results for light-duty vehicles, SAE transactions, 113, 1354–1373, 2004. 15539, 15540

Olivares, G., Johansson, C., Ström, J., and Hanson, H.: The role of ambient temperature for particle number concentrations in a street canyon, Atmos. Env., 41, 2145–2155, 2007. 15563

Palmgren, F., Berkowicz, R., Ziv, A., and Hertel, O.: Actual car fleet emissions estimated from urban air quality measurements and street pollution models, Sci. Tot. Env., 235, 101–109, 1999. 15551

Peters, A., Wichmann, H. E., Tuch, T., Heinrich, J., and Heyder, J.: Respiratory Effects are

Associated with the Number of Ultrafine Particles, Am. J. Respir. Crit. Care Med., 155, 1376–1383, 1997. 15539

Pohjola, M., Pirjola, L., Kukkonen, J., and Kulmala, M.: Modelling of the influence of aerosol processes for the dispersion of vehicular exhaust plumes in street environment, Atmos. Env., 37, 339–351, 2003. 15540

Pope, C. A., Burnett, R. T., Thun, M. J., et al.: Lung cancer, cardiopulmonary mortality, and long-term exposure to fine particulate air pollution, J. Aerosol Med., 287, 1132–1141, 2002. 15538

Rose, D., Wehner, B., Ketzel, M., amd J. Voigtänder, C. E., Tuch, T., and Wiedensohler, A.: Atmospheric number size distributions of soot particles and estimation of emission factors, Atmos. Chem. Phys., 6, 1021–1031, 2006, http://www.atmos-chem-phys.net/6/1021/2006/. 15539

Rosenbohm, E., Vogt, R., Scheer, V., Nielsen, O., Dreiseidler, A., Baumbach, G., Imhof, D., Baltensperger, U., Fuchs, J., and Jaeschke, W.: Particulate size distributions and mass measured at a motorway during the BAB II campaign, Atmos. Env., 39, 5696–5709, 2005. 15540

Samaras, Z., Ntziachristos, L., Thompson, N., Hall, D., Westerholm, R., and Boulter, P.: Characterisation of Exhaust Particulate Emissions from Road Vehicles (PARTICULATES), Web report, Aristotle University of Thessaloniki, Laboratory of Applied Thermodynamics, available at: http://lat.eng.auth.gr/particulates, 2005. 15539, 15540

Schlünzen, K. H., Hinneburg, D., Lambrecht, M., Leitl, B., Lopez, S., Lüpkes, C., Panskus, H., Renner, E., Schatzmann, M., Schoenemeyer, T., Trepte, S., and Wolke, R.: Flow and Tranport in the Obstacle Layer: First Results of the Micro-Scale Model MITRAS, J. Atmos. Chem., 44, 113–130, 2003. 15541

Schwartz, J., Dockery, D., and Neas, L.: Is daily mortality associated specifically with fine particles?, J. Air Waste Manage. Assoc., 46, 927–939, 1996. 15539

Seaton, A., MacNee, W., Donaldson, K., and Godden, D.: Particulate Air Pollution and Acute Health Effects, Lancet, 345, 176–178, 1995. 15539

Seinfeld, J. H. and Pandis, S. P.: Atmospheric Chemistry and Physics: from air pollution to climate change, John Wiley, New York, USA, 2 edition, 1326 p., 1998. 15565

Spurny, K. R.: Analytical chemistry of aerosols, Science and Technology, Lewis, CRC Press, Boca Raton, USA, 486 p., 1999. 15539

Vachon, G., Louka, P., Rosant, J., Mestayer, P., and Sini, J.: Measurements of Traffic-Induced

Turbulence within a Street Canyon during the Nantes'99 Experiment, Water Air Soil Poll., 2, 127–140, 2002. 15559
Vardoulakis, S., Fisher, B., Pericleous, K., and Gonzalez-Flesca, N.: Modelling air quality in street canyons: a review, Atmos. Env., 37, 155–182, 2003. 15540
Voigtländer, J., Tuch, T., Birmili, W., and Wiedensohler, A.: Correlation between traffic density and particle size distribution in a street canyon and the dependence on wind direction, Atmos. Chem. Phys., 6, 4275–4286, 2006, http://www.atmos-chem-phys.net/6/4275/2006/. 15540
Wehner, B., Birmili, W., Gnauk, T., and Wiedensohler, A.: Particle number size distributions in a street canyon and their transformation into the urban background: Measurements and a simple model study, Atmos. Env., 36, 2215–2223, 2002. 15540
Weingartner, E., Keller, C., Stahel, W. A., Burtscher, H., and Baltensperger, U.: Aerosol Emission in a Road Tunnel, Atmos. Env., 31, 451–462, 1997. 15539
Winklmayr, W., Reischl, G. P., Linde, A. O., and Berner, A.: A New Electromobility Spectrometer for the Measurement of Aerosol Size Distributions in the Size Range from 1 to 1000 nm, J. Aerosol Sci., 22, 289–296, 1991. 15543
Wissink, A., Chand, K., Kosovic, B., Chan, S., Berger, M., and Chow, F.: Adaptive Urban Dispersion Integrated Model, presentation at the 86th American Meteorological Society Annual Meeting Atlanta, UCRL-PROC-216813, 21 p., 2005 (downloadable from https://computation.llnl.gov/casc/audim/pube.html) 15541
Zhang, K., Wexler, A., Niemeier, D., Zhud, Y., Hinds, W., and Sioutas, C.: Evolution of particle number distribution near roadways – Part III: Traffic analysis and on-road size resolved particulate emission factors, Atmos Env., 39, 4155–4166, 2005.
Zhang, K. M. and Wexler, A. S.: Evolution of particle number distribution near roadways – Part I: analysis of aerosol dynamics and its implications for engine emission measurement, Atmos Env., 38, 6643–6653, 2004. 15540
Zhang, K. M., Wexler, A. S., Zhu, Y., Hinds, W. C., and Sioutas, C.: Evolution of particle number distribution near roadways – Part II: the "Road-to-Ambient" process, Atmos Env., 38, 6655–6665, 2004. 15562
Zhu, Y. and Hinds, W.: Concentration and Size Distribution of Ultrafine Particles Near a Major Highway, J. Air Waste Manag. Assoc., 52, 1032–1042, 2002.
15540

Table 1. Number of vehicles on the A100 motorway, average between 28 June and 6 August 2005.

	night (21–05 h)		day (05–21 h)		in 24 h	
	car-like	lorry-like	car-like	lorry-like	car-like	lorry-like
Mon–Fri	18 400	900	151 200	10 200	169 600	11 100
Sat	21 400	600	111 600	4 000	133 000	4 600
Sun	20 500	500	100 600	2 600	121 100	3 100

ACPD
8, 15537–15594, 2008

Table 2. Lognormal modal parameters of the number size distributions at at the roadside and background sites. D_{g0} indicates mean geometric diameter, N modal number concentration in cm^{-3}, and σ the geometric spread parameter.

	Young Aitken mode (σ=1.70)			Aitken mode (σ=1.58)			Accumulation mode (σ=1.59)		
Perc.	D_{g0} in nm	N (roads.)	N (backg.)	D_{g0} in nm	N (roads.)	N (backg.)	D_{g0} in nm	N (roads.)	N (backg.)
25	18	5 400	2 300	53	3 800	1 600	134	1 800	1 100
50	18	14 000	4 000	58	8 000	2 300	138	2 900	1 500
75	18	32 000	6 700	65	15 000	3 500	147	3 900	2 000
95	18	81 000	14 000	74	28 000	6 500	168	4 400	3 100
99	18	140 000	24 000	81	39 000	11 000	208	3 400	2 600

ACPD
8, 15537–15594, 2008

Table 3. Variables used in the modelling part, with their SI units, and the units used here.

variable	description	physical units SI	this paper
U	large-scale wind speed	$m\,s^{-1}$	$m\,s^{-1}$
u	local wind speed	$m\,s^{-1}$	$m\,s^{-1}$
u^*	local wind speed (normalised)	1	1
c	particle number concentration	m^{-3}	cm^{-3}
c^*	particle number concentration (normalised)	1	1
h	height of the modelling domain	m	m
H	characteristic obstacle height	m	m
Q	line source intensity	$m^{-1}\,s^{-1}$	$m^{-1}\,s^{-1}$
M	traffic density	(veh.) s^{-1}	(veh.) s^{-1}
F	dilution factor	$s\,m^{-2}$	$s\,m^{-2}$
η	scaling constant	1	1
E_N	particle number emission factor (veh.$^{-1}$)	m^{-1}	km^{-1}
E_V	particle volume emission factor (veh.$^{-1}$)	$m^3\,m^{-1}$	$cm^3\,km^{-1}$

ACPD
8, 15537–15594, 2008

Table 4. Simulated wind direction, normalised wind speed (u^*) and particle concentrations (c^* and c^*u^*) at the positions of the roadside and background measurement sites. The calculations refer to 10 discrete directions of the driving large scale wind ($U = 10\,\mathrm{m\,s^{-1}}$) at h=100 m.

	roadside site "C"				background site "T"			
large scale wind dir.	simulated wind wind dir.	u^*	simulated concentrations c^*	c^*u^*	simulated wind wind dir.	u^*	c^*	c^*u^*
0°	5°	0.37	18.2	6.7	0°	0.30	0	0
45°	26°	0.52	32.6	16.9	30°	0.25	0	0
90°	58°	0.39	18.9	7.4	96°	0.33	0	0
135°	145°	0.22	21.3	4.7	110°	0.27	0	0
180°	225°	0.55	0	0	174°	0.33	5.0	1.7
225°	258°	0.50	0.13	0.06	219°	0.28	6.5	1.8
270°	36°	0.06	65.7	3.9	264°	0.46	8.4	3.9
292°	55°	0.10	59.4	5.9	324°	0.30	3.4	1.0
315°	20°	0.15	44.9	6.7	313°	0.34	4.0	1.4
338°	5°	0.26	8.2	2.1	343°	0.31	0.28	0.09

ACPD
8, 15537–15594, 2008

Table 5. Particle number emission factors (particle size range: 10–500 nm) for the A100 motorway using the three calculation approaches in 10^{14} veh^{-1} km^{-1}.

E based on c(roadside)-c(background)			
period (LT)	Eq. 6	Eq. 8	Eq. 9
01:00–07:00	2.81 (0.71)	2.83 (0.22)	2.16 (0.23)
07:00–14:00	1.85 (0.21)	2.49 (0.25)	1.85 (0.37)
14:00–21:00	1.18 (0.14)	1.48 (0.16)	1.17 (0.14)

ACPD
8, 15537–15594, 2008

Table 6. Comparison of emission factors from the literature and this work. Emphasis is directed towards values representative for roads with free-flowing traffic and travelling speeds of 80 km h^{-1} and greater. Uncertainties are indicated in brackets.

Study	D_p range[a]	speed[b]	vehicle type[c]	method	E_N[d]	E_V[e]	distance[f]
Mixed fleet results							
Abu-Allaban et al. (2002)	10–400	< 90	47–85%	tunnel	2.10–3.13		n.a.
Imhof et al. (2005)	7–300	120	ca. 18%	NO_x	11.7	0.027	20–25 m
Imhof et al. (2005)	7–300	80–100	ca. 18%	NO_x	13.5	0.048	8–20 m
Hueglin et al. (2006)	7–1000	100	18%	NO_x	7.9		20 m
Imhof et al. (2006)	18–700	80	18%	tunnel	1.50 (0.08)	0.21 (0.008)	n.a.
Abu-Allaban et al. (2002)	10–400	< 90	14%	tunnel	0.52–0.54		n.a.
Gramotnev et al. (2003)	15–700	100	14%	Gaussian	2.8 (0.3)		15 m
this work	10–500	75–90	6%	CFD	2.1 (0.2)	0.077 (0.01)	6 m
this work	soot mode	75–90	6%	CFD	1.5 (0.2)	0.17 (0.02)	6 m
this work	nucleation mode	75–90	6%	CFD	3.3 (0.3)	0.003 (0.001)	6 m
Zhang et al. (2005)	6–220	85	5.5%	CO	1.0–4.7		n.s.
Corsmeier et al. (2005)	30–300	85–110	4.8%	box model	1.8		3 m
Kristensson et al. (2004)	3–900	70–90	4.5%	tunnel	4.6 (1.9)		n.a.
Morawska et al. (2005)	15–700	100	4%	box model	1.11 (0.9)		bridge
Janhäll and Hallquist (2005)	10–400	92	n.s.	NO_x	35 (15)[g]		n.s.
HDV fraction results							
Imhof et al. (2005)	7–300	120	HDV	NO_x	73	0.239	20-25 m
Imhof et al. (2005)	7–300	80-100	HDV	NO_x	69	0.19	8-20 m
Morawska et al. (2005)	15–700	100	HDV	box model	7.17 (2.8)		bridge
Corsmeier et al. (2005)	30–300	85	HDV	box model	7.8	0.41	3 m
this work	10–500	75–90	HDV	CFD	10 (1.5)		6 m
LDV fraction results							
Imhof et al. (2005)	7–300	120	LDV	NO_x	6.9	0.013	20–25 m
Imhof et al. (2005)	7–300	80–100	LDV	NO_x	3.2	0.021	8–20 m
Morawska et al. (2005)	15–700	100	LDV[h]	box model	0.19 (3.40)		bridge
Corsmeier et al. (2005)	30–300	85	LDV	box model	1.22	0.03	3 m
this work	10–500	75–90	LDV	CFD	0.09 (0.06)		6 m

n.a. = not applicable. n.s. = not specified.
[a] in nm. [b] in km h^{-1}. [c] fraction of HDVs in a mixed fleet unless specified. [d] in 10^{14} veh^{-1} km^{-1}.
[e] in 10^{14} cm^3 veh^{-1} km^{-1}. [f] of the sampling point from the road. [g] per mol NO_x. [h] almost only gasoline cars.

ACPD
8, 15537–15594, 2008

Table 7. Calculated life times of 18 nm-particles against Brownian coagulation. The size distributions refer to different percentiles of the aerosol sampled at the roadside site. $D_{p,\max}$ is the diameter of the pre-existing particle population that contributes most to the coagulation rate. Two hygroscopic particle growth factors (GF) are intended to simulate dry and humid conditions.

			dry ambient conditions (GF=1)			dry ambient conditions (GF=1.4)		
Size distribution	Total N	$D_{p,\max}$	$t_{0.90}$	$t_{0.75}$	$t_{0.50}$	$t_{0.90}$	$t_{0.75}$	$t_{0.50}$
Perc. 50	20 000 cm^{-3}	89 nm	36 min	98 min	240 min	24 min	65 min	158 min
Perc. 75	52 000 cm^{-3}	89 nm	19 min	52 min	120 min	13 min	34 min	83 min
Perc. 95	110 000 cm^{-3}	91 nm	10 min	26 min	63 min	6 min	17 min	41 min
Perc. 99	180 000 cm^{-3}	96 nm	6 min	18 min	43 min	4 min	12 min	28 min
Perc. 99, YA$\star$ 10	1 400 000 cm^{-3}	18 nm	2 min	4 min	11 min	1 min	3 min	6 min

ACPD
8, 15537–15594, 2008

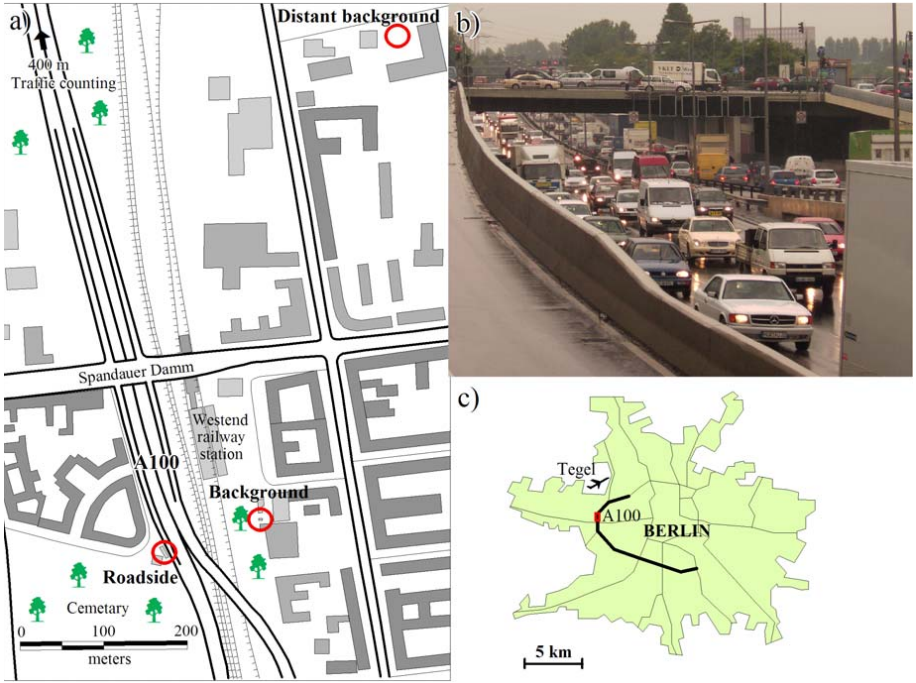

Fig. 1. **(a)** Location of the measurement and traffic count sites near the motorway A100. **(b)** Traffic on the motorway near Spandauer Damm bridge. **(c)** Location of the motorway and Tegel Airport in Berlin.

ACPD
8, 15537–15594, 2008

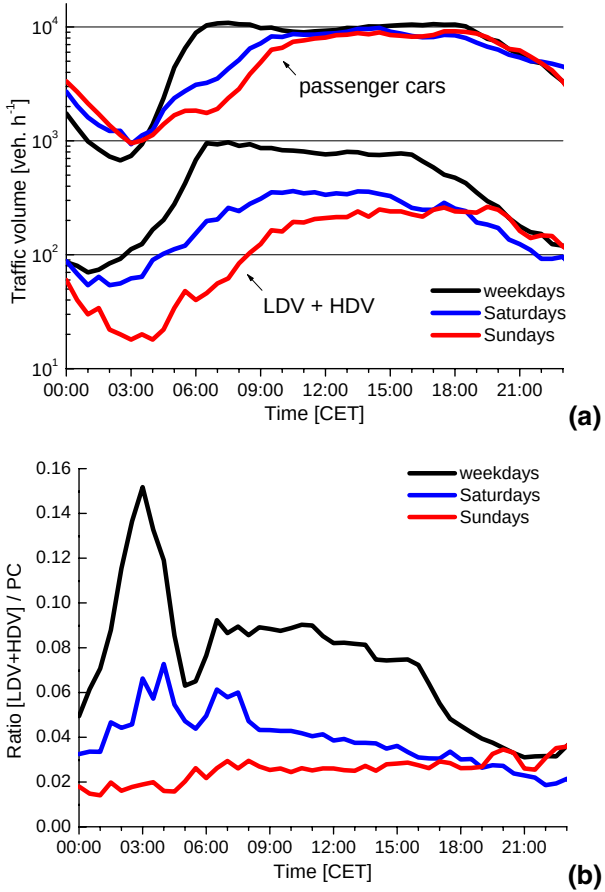

Fig. 2. Traffic parameters on the A100 motorway: **(a)** Diurnal cycle of traffic volume for passenger cars and lorry-like vehicles (light plus heavy duty vehicles). **(b)** the ratio between lorry-like vehicles and passenger cars.

ACPD
8, 15537–15594, 2008

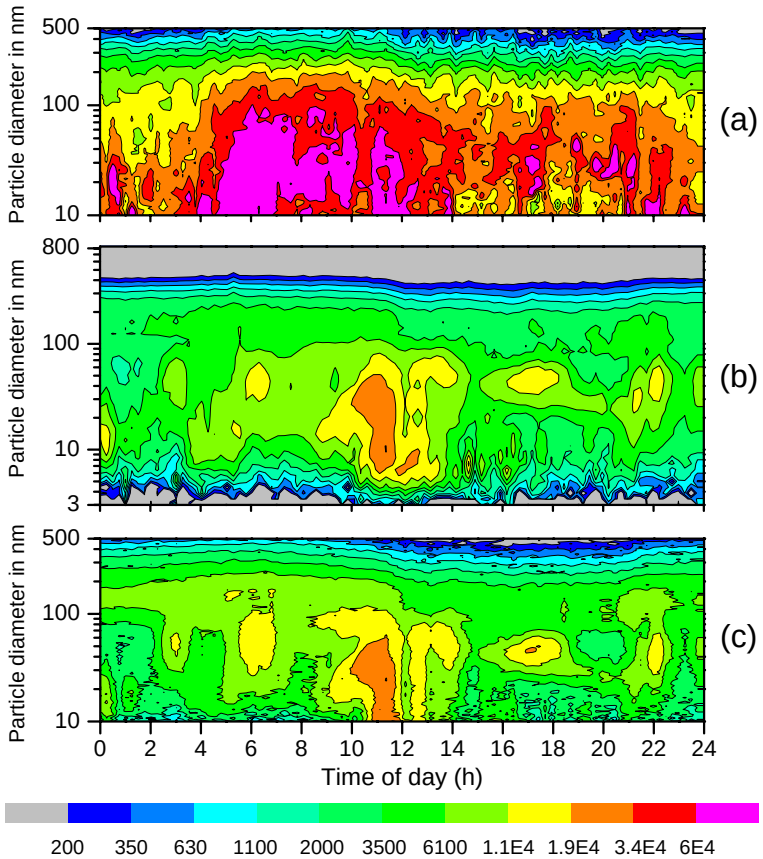

Fig. 3. Particle number size distributions ($dN/dlogD_p$ in cm^{-3}) at the three urban measurement sites on 12 July 2005: **(a)** roadside, **(b)** background, **(c)** distant background.

ACPD
8, 15537–15594, 2008

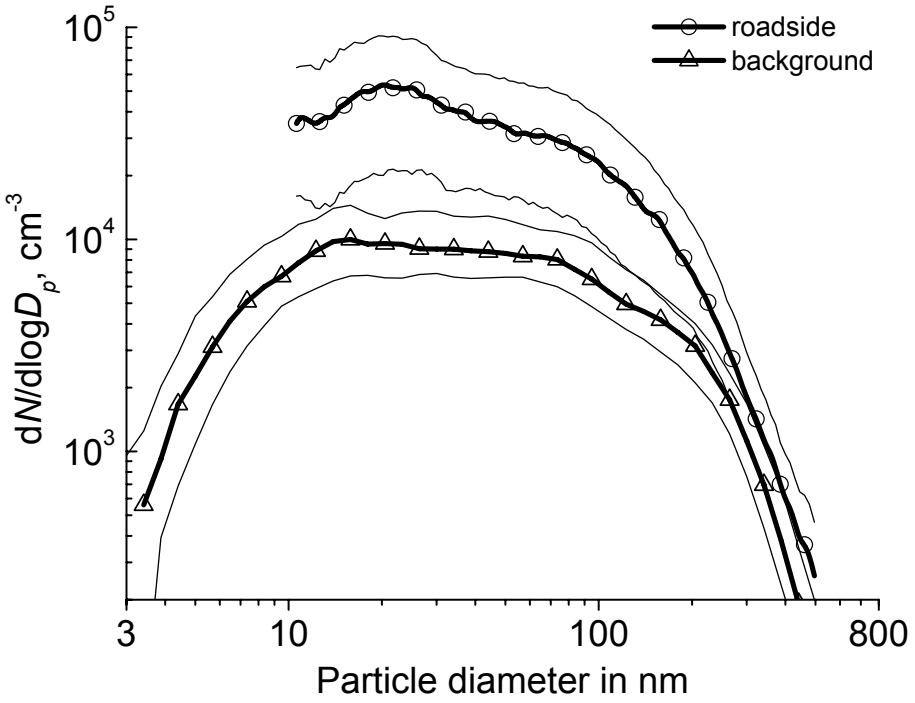

Fig. 4. Median particle number size distributions at roadside and in the urban background during peak traffic hours (07:00–09:00 local time). The thin lines correspond to the 25th and 75th percentile distributions.

ACPD

8, 15537–15594, 2008

Traffic-related exhaust particles near the Berlin urban motorway

W. Birmili et al.

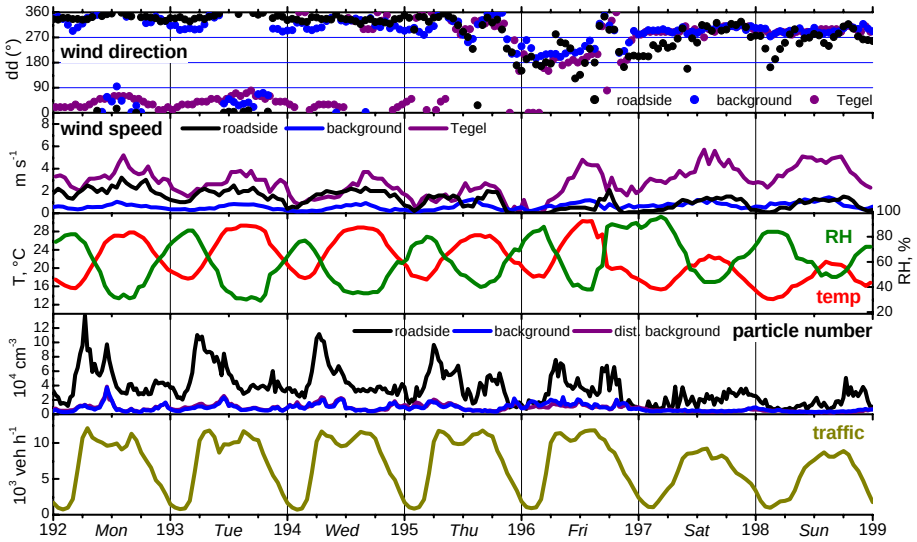

Fig. 5a. Meteorological, particle and traffic parameters near the A100 motorway during one-week case studies: **(a)** 11–17 July 2005.

ACPD
8, 15537–15594, 2008

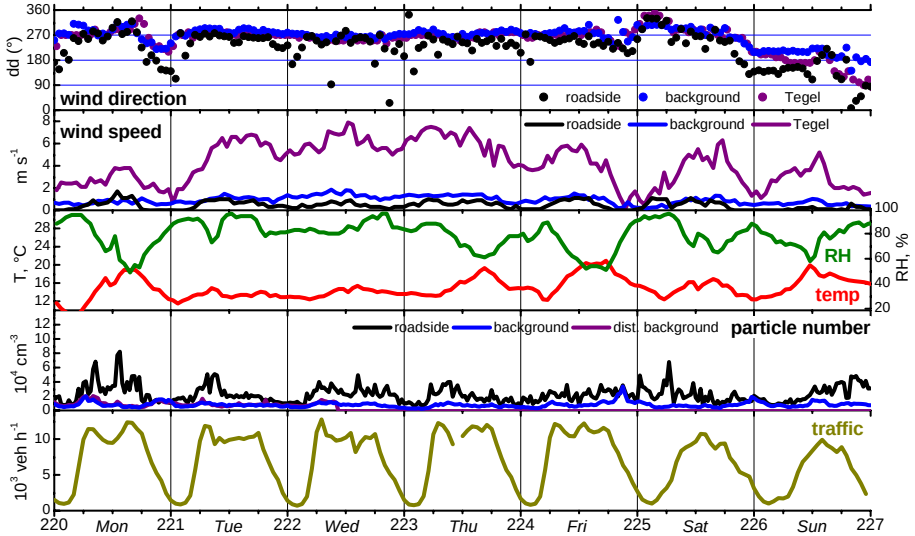

Fig. 5b. Meteorological, particle and traffic parameters near the A100 motorway during one-week case studies: **(b)** 8–14 August 2005.

ACPD
8, 15537–15594, 2008

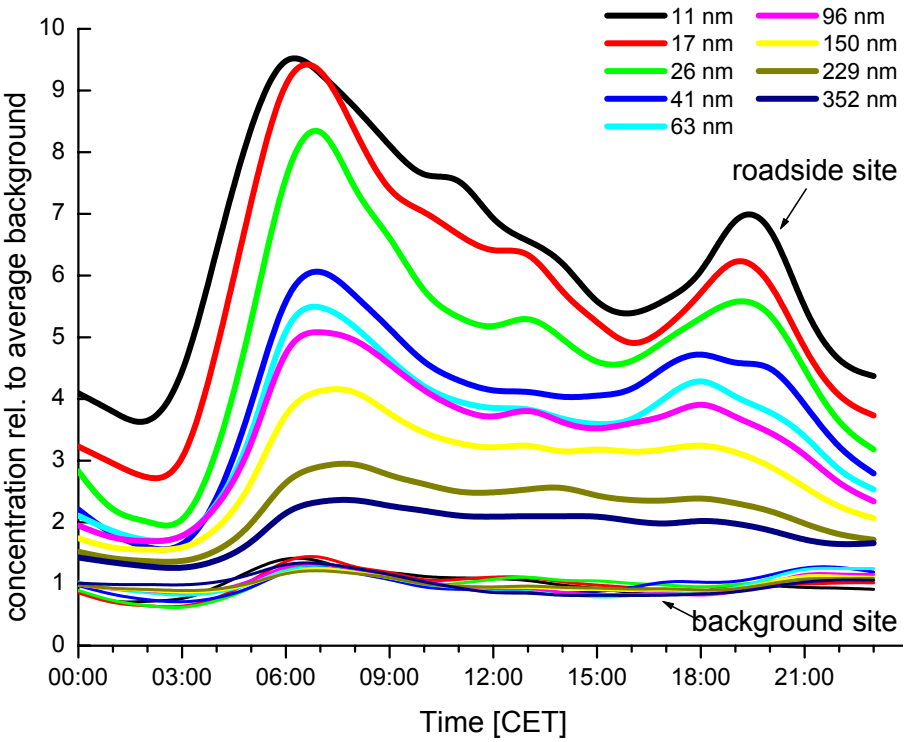

Fig. 6. Average diurnal cycles for particle number concentrations on workdays. Concentrations are indicated for a selection of particle diameters at the roadside and background sites, respectively, as a function of the average levels at the background site.

ACPD
8, 15537–15594, 2008

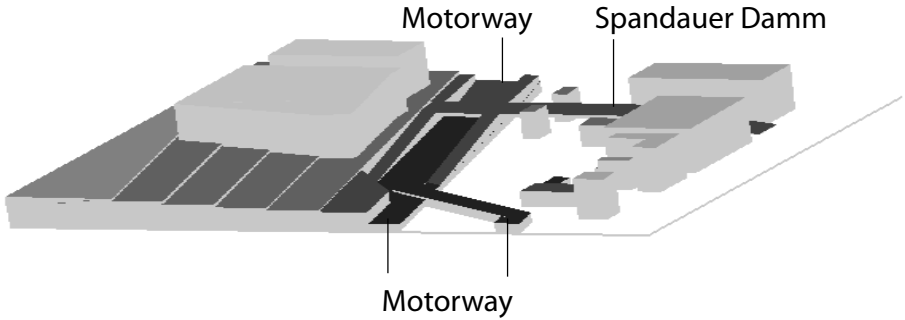

Fig. 7. 3-D model domain with the A100 motorway in black.

ACPD
8, 15537–15594, 2008

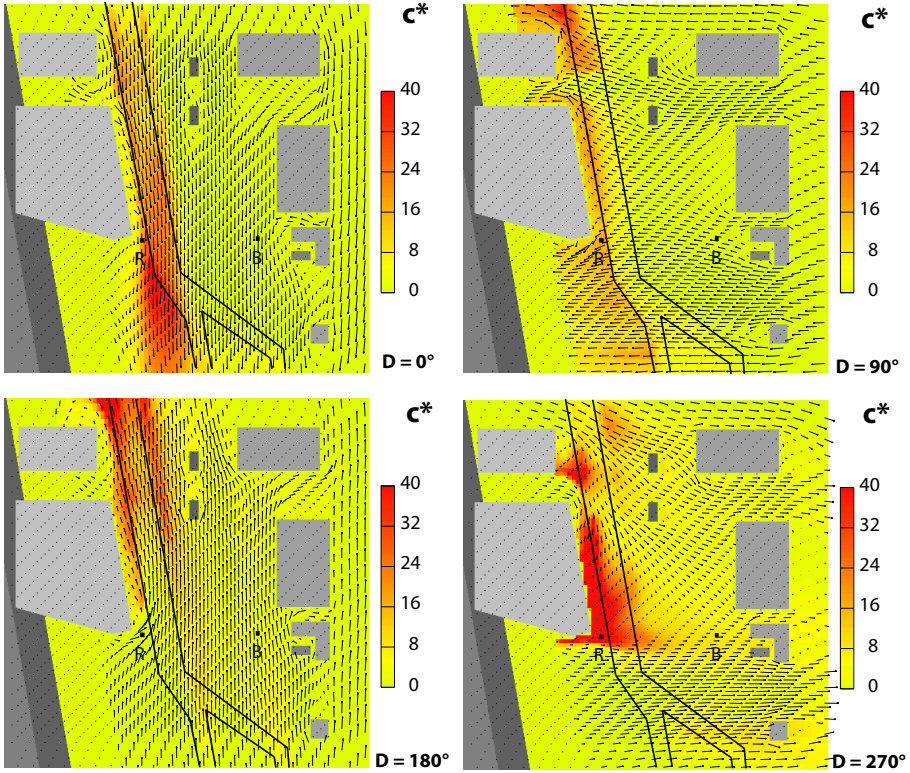

Fig. 8. Wind field and normalised concentrations in the layer of the height of the roadside site (C) for driving wind from north ($D = 0^{\circ}$), east ($D = 90^{\circ}$), south ($D = 180^{\circ}$), and west ($D = 270^{\circ}$).

ACPD
8, 15537–15594, 2008

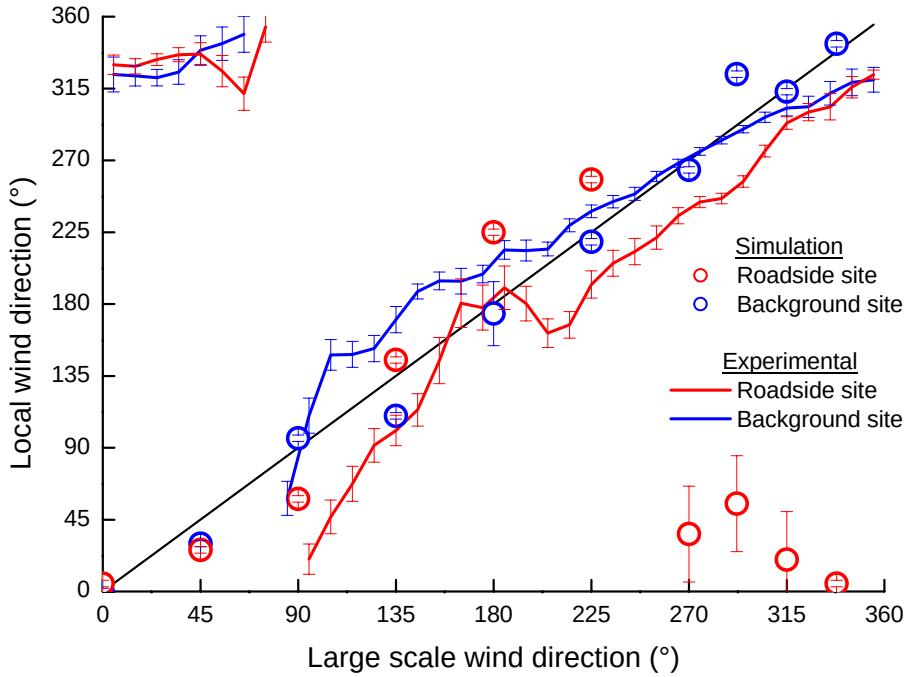

Fig. 9a. Comparison of simulated and experimental wind as a function on the large scale wind direction: **(a)** wind direction.

ACPD

8, 15537–15594, 2008

Traffic-related exhaust particles near the Berlin urban motorway

W. Birmili et al.

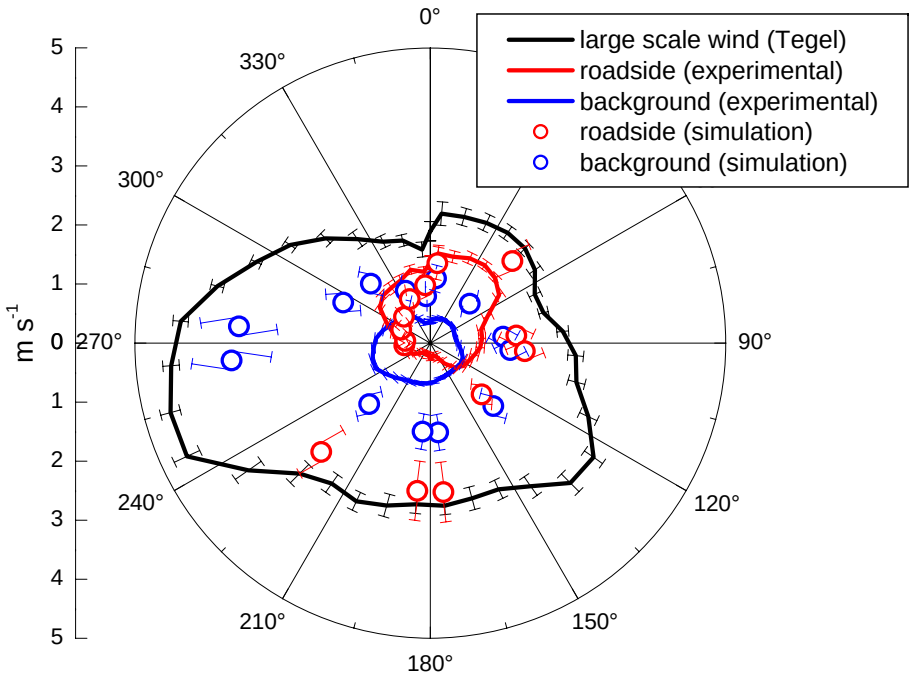

Fig. 9b. Comparison of simulated and experimental wind as a function on the large scale wind direction: **(b)** wind speed.

ACPD

8, 15537–15594, 2008

Traffic-related exhaust particles near the Berlin urban motorway

W. Birmili et al.

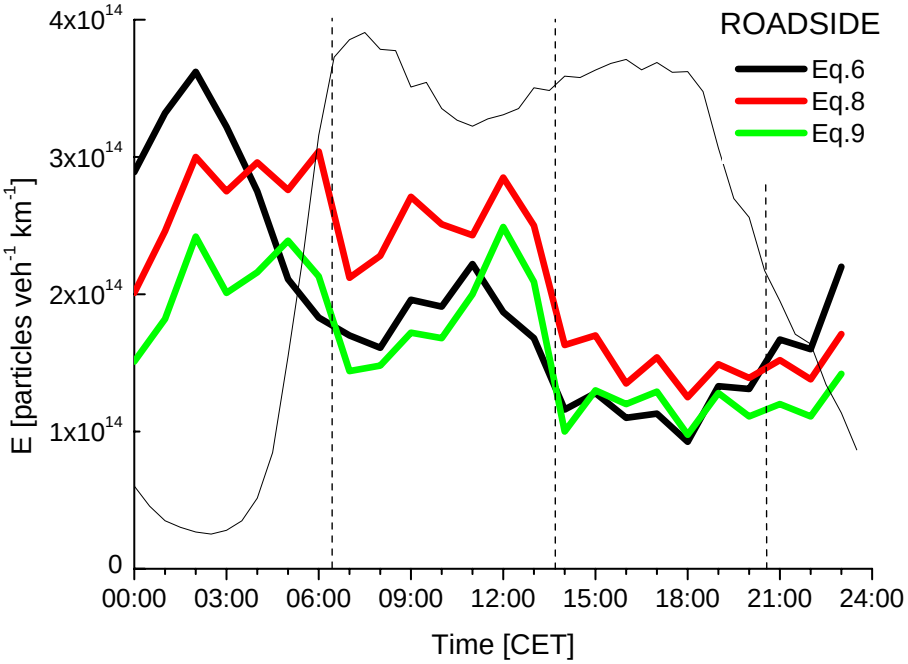

Fig. 10a. Diurnal cycles of the fleet emission factor based on **(a)** roadside minus background measurements using the three different calculation approaches. Vertical lines delimit the time periods evaluated in Sect. 5.1. The total traffic volume (without units) appears as a thin line.

ACPD
8, 15537–15594, 2008

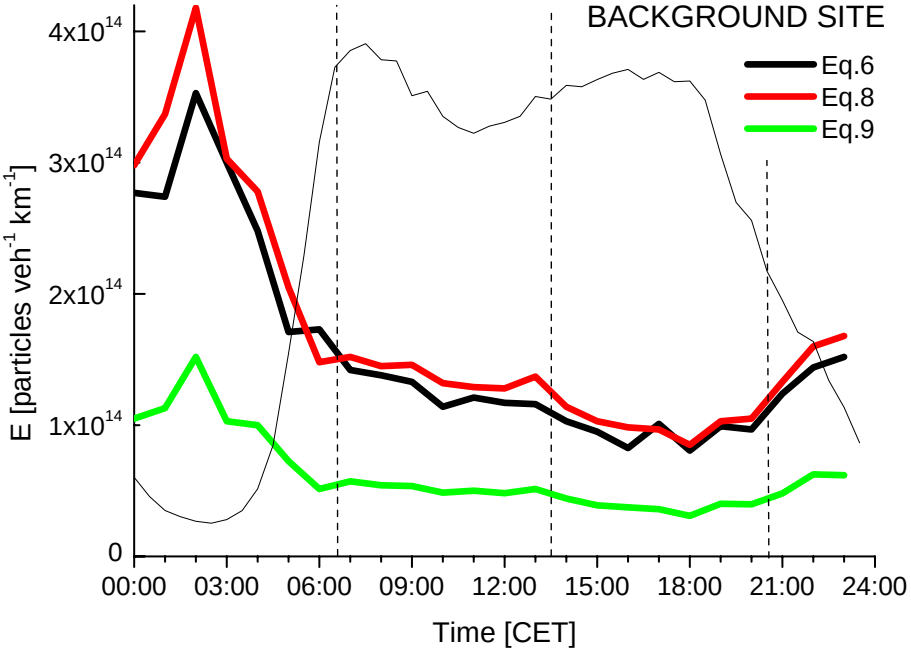

Fig. 10b. Diurnal cycles of the fleet emission factor based on **(b)** background measurements only using the three different calculation approaches. Vertical lines delimit the time periods evaluated in Sect. 5.1. The total traffic volume (without units) appears as a thin line.

ACPD
8, 15537–15594, 2008

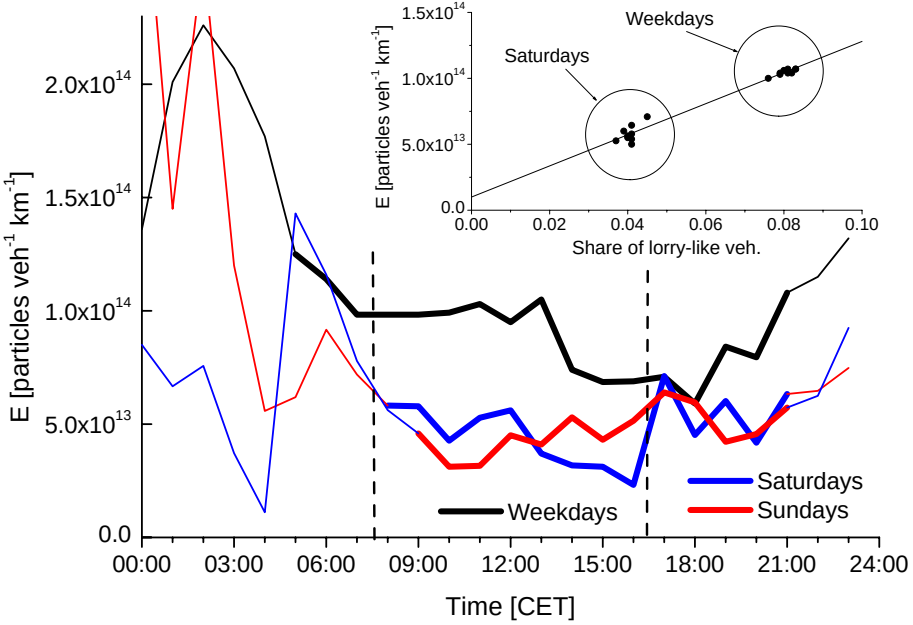

Fig. 11. Diurnal profiles of the emission factor E at the roadside site for different times of the week using Eq. 8. Dashed lines delimit the range of reliable data. Inset: Correlation analysis for E as a function of the relative share of lorry-like vehicles in the fleet.

ACPD
8, 15537–15594, 2008

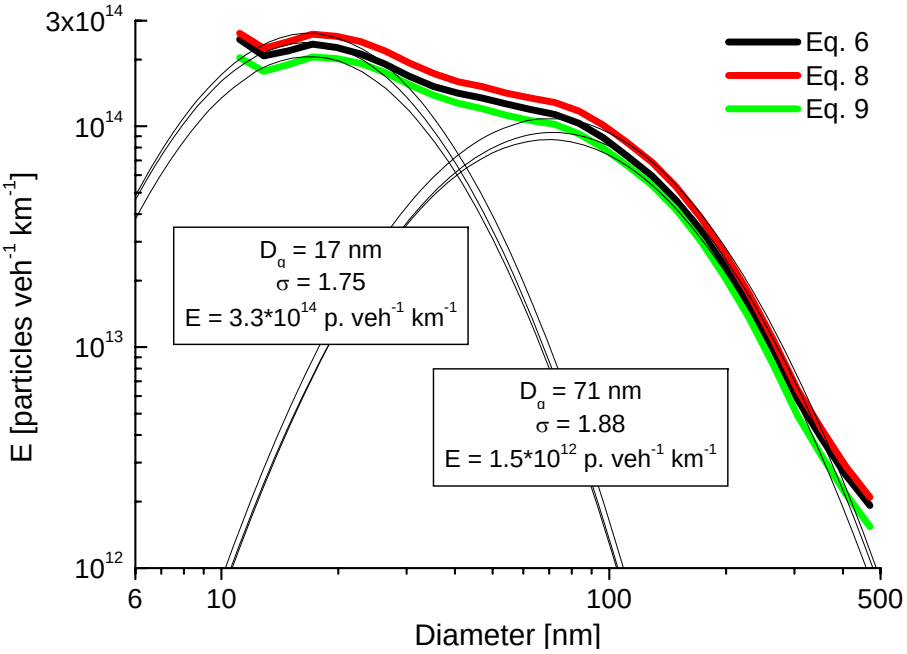

Fig. 12. Size distribution $dE/d\lg D_p$ of the number emission factor based on roadside data using the three calculation approaches. Lognormal modal parameters are indicated for Eq. 8.

ACPD

8, 15537–15594, 2008

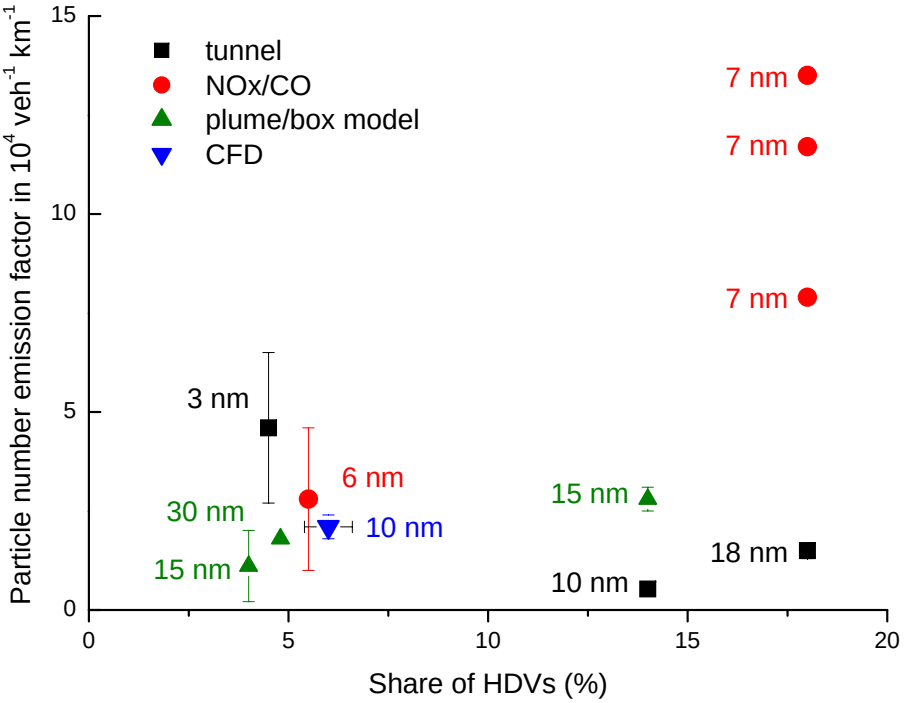

Fig. 13. Compilation of fleet emission factors of particle number as a function of the relative share of HDVs (studies since 2002). Indicated is the lower cut-off diameter of the particle number concentration measurement.

ACPD
8, 15537–15594, 2008